

# Deciphering the role of solar-induced thermal stresses in rock weathering

Martha Cary Eppes<sup>1,†</sup>, Brian Magi<sup>1</sup>, Bernard Hallet<sup>2</sup>, Eric Delmelle<sup>1</sup>, Peter Mackenzie-Helnwein<sup>3</sup>, Kimberly Warren<sup>4</sup>, and Suraj Swami<sup>1</sup>

<sup>1</sup>Department of Geography and Earth Sciences, University of North Carolina at Charlotte, Charlotte, North Carolina 28223, USA

<sup>2</sup>Department of Earth and Space Sciences, University of Washington, Seattle, Washington 98195, USA

<sup>3</sup>Department of Civil and Environmental Engineering, University of Washington, Seattle, Washington 98195, USA

<sup>4</sup>Department of Civil and Environmental Engineering, University of North Carolina at Charlotte, Charlotte, North Carolina 28223, USA

## ABSTRACT

A dearth of direct field observations limits our understanding of individual mechanical weathering processes and how they interact. In particular, the specific contributions of solar-induced thermal stresses to mechanical weathering are poorly characterized. Here, we present an 11 mo data set of cracking, using acoustic emissions (AEs), combined with measurements of rock temperature, strain and other environmental conditions, all recorded continuously for a granite boulder resting on the ground in open sun. We also present stresses derived from a numerical model of the temperature and stress fields in the boulder, idealized as a uniform elastic sphere experiencing simple solar temperature forcing. The thermal model is validated using this study's data.

Most observed cracking coincides with the timing of calculated maximum, insolation-driven, tensile thermal stresses. We also observe that most cracking occurs when storms, or other weather events, strongly perturb the rock surface temperature field at these times. We hypothesize that these weather-actuated thermal perturbations result in a complex thermal stress distribution that is superimposed on the background stresses arising from simple diurnal forcing; these additive stresses ultimately trigger measurable cracking. Measured locations of observed cracking and surface strain support this hypothesis in that they generally match model-predicted locations of maximum solar-induced tensile stresses. Also, recorded rock surface strain scales with diurnal temperature cycling and records progressive, cumulative extension (dilation), consistent with ongoing, thermal stress-driven subcriti-

cal crack growth in the boulder.

**Our results therefore suggest that (1) insolation-related thermal stresses by themselves are of sufficient magnitude to facilitate incremental subcritical crack growth that can subsequently be exploited by other chemical and physical processes and (2) simple insolation can impart an elevated tensile stress field that makes rock more susceptible to cracking triggered by added stress from other weathering mechanisms. Our observed cracking activity does not correlate simply with environmental conditions, including temperature extremes or the often-cited 2 °C/min thermal shock threshold. We propose that this lack of correlation is due to both the ever-varying ambient stress levels in any rock at Earth's surface, as well as to the fact that ongoing subcritical crack growth itself will influence a rock's stress field and strength. Because similar thermal cycling is universally experienced by subaerially exposed rock, this study elucidates specific mechanisms by which solar-induced thermal stresses may influence virtually all weathering processes.**

## INTRODUCTION

Understanding the factors that control the mechanisms and rates of rock breakdown is fundamental to interpreting and predicting landscape evolution, as well as interactions among the global lithosphere, biosphere, and atmosphere (e.g., Kirchner et al., 2006; Larsen et al., 2014; Schlesinger and Bernhardt, 2013); however, the specific processes that dominate physical weathering in any given environment are poorly defined and understood. The relative contributions and interactions of different environmental factors like moisture or

temperature are poorly identified because of the dearth of data that could be used to differentiate them, despite a substantial number and diversity of weathering studies (e.g., Anderson, 1998; Gómez-Heras et al., 2006; Hall and Hall, 1996; Moores et al., 2008; Stock et al., 2012; Viles et al., 2010; Yaalon, 1970). Thus, there are numerous testable hypotheses associated with individual weathering processes like ice segregation (e.g., Hales and Roering, 2007; Hallet et al., 1991), salt weathering (e.g., Grossi et al., 2011), or thermal shock (e.g., Boelhouwers and Jonsson, 2013), but we have yet to elucidate an unequivocal link between rock breakdown and the dominant underlying mechanism(s) that drives it in natural settings. Before we can identify the conditions under which mechanical weathering drives or limits overall landscape change on Earth's surface, these links must be documented.

In particular, the role of the sun in rock breakdown through purely thermo-mechanical stressing associated with diurnal temperature forcing continues to be actively debated (e.g., reviews in Boelhouwers and Jonsson, 2013; Goudie, 2013; Hall and Thorn, 2014). The dispute stems from substantial evidence for and against insolation-related thermomechanical stresses being important (e.g., Gómez-Heras et al., 2006; Griggs, 1936; McFadden et al., 2005). These considerations of the role of solar-induced weathering should not be confused, however, with discussions regarding the sun's additional contribution to weathering through its inherent influence on both temperature-related processes like freezing and on temperature-related factors like moisture content. In this paper, we focus on solar-induced thermomechanical stresses, not these other factors.

The thermal stresses that arise in rock due to diurnal insolation are generally thought to be

<sup>†</sup>meppes@uncc.edu

relatively small (e.g., Holzhausen, 1989) and inherently complex, predicated on numerous rock and environmental conditions such as rock size, shape, composition, grain size, location, or even translucence (e.g., Eppes and Griffing, 2010; Gómez-Heras et al., 2006; Hall et al., 2010; Leask and Wilson, 2003; McFadden et al., 2005). Moreover solar-related thermal stresses in any given rock are spatio-temporally complex, and we note that they occur on two distinct length scales—one arising from well-described mechanical interactions between adjacent mineral grains in polycrystalline rocks due to differences in their orientation and thermal and elastic properties (hereafter grain-scale thermal stresses; e.g., Molaro and Byrne, 2015), and the other, the focus of this study, represented by stresses that ensue at the scale of a boulder or bedrock outcrop due to differential heating of the entire rock mass (hereafter macroscale thermal stresses; e.g. Tanigawa and Takeuti, 1983). There is no doubt that these thermal stresses arise daily in any given surface or near-surface rock. The primary lingering questions are to what extent, and by what specific mechanism(s) do these relatively small but omnipresent solar-induced thermal stresses contribute to the breakdown of rock at Earth's surface? We hypothesize that the answer lies in considerations of subcritical crack propagation.

The strength of brittle materials is strongly dependent on preexisting heterogeneities that concentrate stress. Rocks inherently contain such defects in the form of microfractures, pores, and/or grain boundaries, all of which can grow into larger fractures that propagate over long time scales, under tensile stresses that are much lower than the laboratory-measured tensile strength of the rock sample (i.e., subcritical crack growth—e.g., Atkinson, 1984, 1987; a.k.a. static fatigue or time-dependent fracture—Brantut et al., 2013). Thus, we hypothesize that mechanical weathering proceeds in all rocks progressively, albeit slowly, under relatively modest stresses. Subcritical crack growth has only very rarely been considered in the context of surface or near-surface processes (e.g., Stock et al., 2012; Walder and Hallet, 1985), despite the fact that the geological time scales of exposure of Earth's rocks likely provide ample time for subcritical crack growth to cause measurable rock breakdown.

The lower stress limit,  $K_{th}$ , for subcritical crack growth is poorly known, but is thought to be within ~10%–20% of any given rock's critical fracture toughness ( $K_c$ , the stress beyond which a material containing a fracture of a given length will catastrophically crack; e.g., Brantut et al., 2013; Meredith and Atkinson, 1985). Thus, we posit that solar-induced

thermal stresses are generally sufficient to produce subcritical crack growth in rocks at Earth's surface. In turn, we hypothesize that these thermal stresses might influence other mechanical weathering processes, in that (1) they lower the overall strength of the rock by lengthening pre-existing cracks and increasing microfracture-related porosity, and, (2) they contribute to crack propagation by other synchronous stressing mechanisms, because they are additive.

To test these hypotheses, we developed a multisensor instrumentation system designed specifically to monitor crack growth using acoustic emissions (AEs) for a granite boulder placed on the ground surface with full sun exposure in North Carolina, United States (Warren et al., 2013). AE data were used to monitor crack growth activity in the boulder continuously through time, along the lines of other AE studies (Grosse and Ohtsu, 2008; Lockner, 1993). We also measured the boulder's surface and environmental conditions for ~1 yr. Using this system, we minimized effects complicating the state of stress that are common in natural settings, such as proximity to preexisting joints and topographic stresses, as well as influences of biological processes and/or moisture retention by adjacent soil or vegetative cover. As such, the effects of simple solar thermal forcing in cracking the boulder could be isolated and examined closely.

Using this data set, combined with a numerical model of macroscale thermal stresses that was developed using this study's temperature data as validation, we begin to discern the conditions under which thermal mechanical stresses arising from simple insolation lead to crack propagation. (Hereafter, we use the term "simple solar forcing" to refer to rock temperature variations and the associated thermo-mechanical stresses brought on solely through diurnal insolation, not weather such as rain or wind.) Our results suggest that this simple recurrent diurnal forcing results in cracking that is accelerated by additive thermal stresses brought on by weather. Because temperature cycling similar to that measured herein is ubiquitous at Earth's surface, our results have important implications for the way in which simple solar forcing may enhance weathering in general, by growing microfractures and aiding other stress-inducing processes in environments worldwide.

## METHODS

### The Boulder

The rock selected for this study is a granite boulder collected from the southern flank of the

San Bernardino Mountains in Southern California (34.101°N, 117.105°W; Fig. 1), hereafter referred to as "the boulder" or "the rock." It is 0.34 m long, 0.25 m wide, 0.24 m high, and ellipsoid in shape (Fig. 1), and it is composed of coarse-grained (average grain diameter 1–5 mm), nonfoliated, and nonporphyritic, hornblende-biotite granodiorite likely from the Cretaceous Granodiorite of Angel Oakes (Morton et al., 2006).

The boulder was collected from an unvegetated gravel bar in a dry wash in a semiarid environment. Such a clast is likely to be episodically tumbled in the channel, causing breaking along any major inherited crack, and it would have remained relatively dry most of the time. When collected, the chosen boulder appeared sound mechanically, with no obvious cracks, other than those found in a "dimple" on its western (as ultimately deployed) side. The boulder was stored in climate controlled conditions for approximately 1 yr prior to installation in the field.

### Instrumentation Overview

The timing and location of rock cracking in the boulder were monitored continuously by six AE sensors for 11 mo. Hereafter, we use the term cracking to refer to any fracture activity that generated AEs; this includes any fracture formation or propagation events that were sufficiently energetic for our sensors to discern. This detection energy threshold is dictated by the specific AE system employed for monitoring. With the somewhat robust intermediate-frequency sensitivity and setup of our AE system (see following), the "cracking" that we refer to herein is not the splitting of the boulder, but instead represents miniscule, incremental growth of fractures, the accumulation of which, over much longer time scales than that of this study, would ultimately result in rock breakup.

Ambient weather conditions, rock surface temperature, strain, and moisture were also measured on the boulder surface in several locations once every minute. Although, higher-frequency surface and environmental data may provide key insights into cracking processes (Hall and André, 2003; McKay et al., 2009), the 60 s resolution was practically optimal for this study given its long duration and the number of sensors being monitored.

The instrumentation affixed to the surface of the boulder consisted of eight thermocouples, eight strain gauge rosettes, six AE sensors, and one surface moisture sensor (Fig. 1). Sensors were not placed in the interior of the boulder to minimize artificial heterogeneities introduced during the installation process that

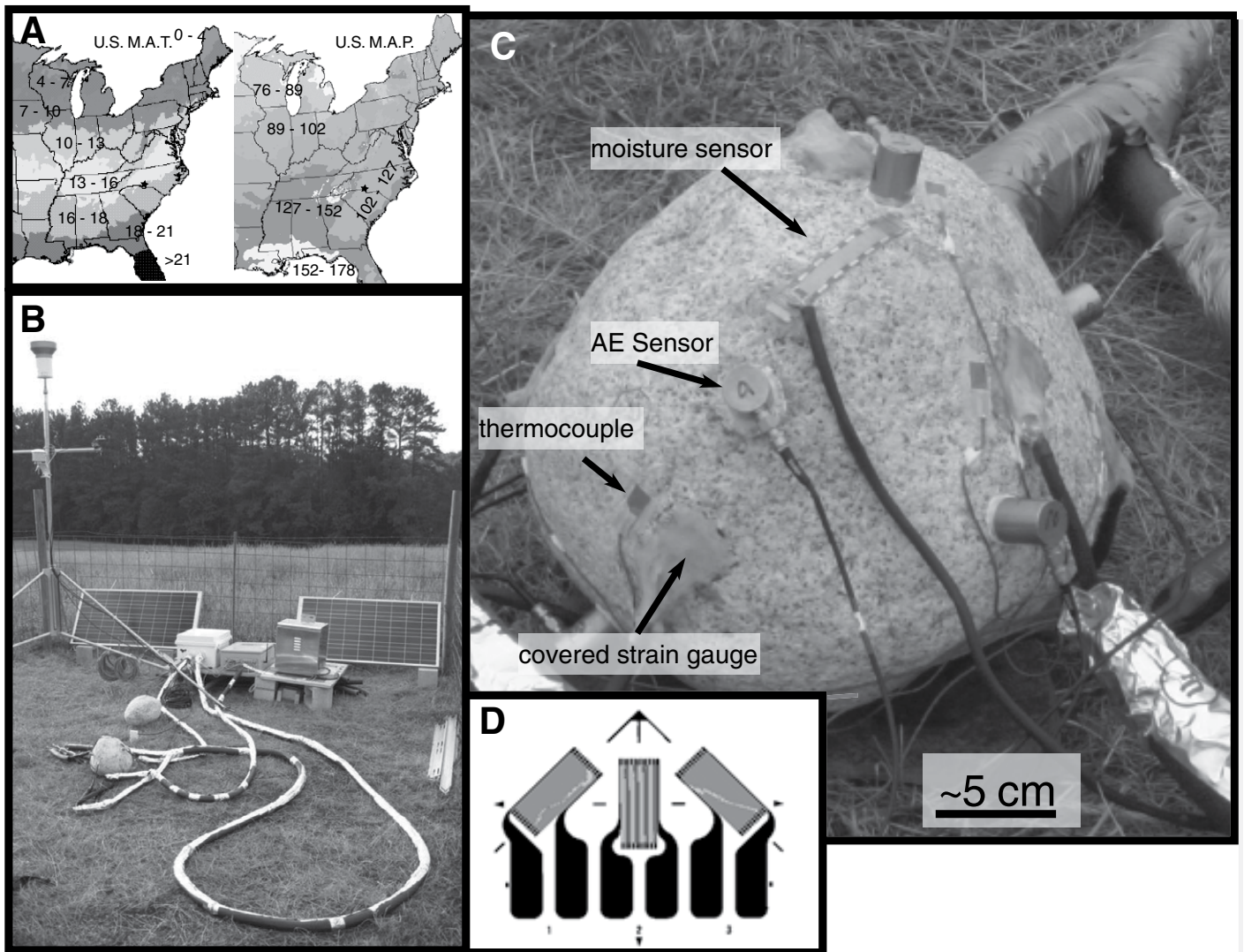


**Figure 1.** Modified from Warren et al. (2013). (A) Field site location (star) at 35°17'55"N, 81°05'17"W, elevation 235 m, that has been superimposed on maps (National Oceanic and Atmospheric Administration and OCS [Oregon Climate Service]) of mean annual temperature (MAT, °C) and mean annual precipitation (MAP, cm). (B) The instrumented granite boulder on site near Charlotte, North Carolina. The study boulder is in the front of the photo. (C) The instrumented boulder with representative sensors noted. AE—acoustic emissions. (D) A schematic of the 3 gauge rosette strain gauge used for this study.

might act as foci for stresses and subsequent fracture. The six AE sensors were positioned on the boulder to minimize errors associated with locating the foci of AE events (Fig. 1). All sensors were installed on the boulder and calibrated in a controlled laboratory environment prior to field deployment. The following sections briefly describe the instrumentation; the details of installation and calibration procedures have been more fully described by Warren et al. (2013).

### Measuring AEs as a Proxy for Rock Cracking

AEs are transient elastic waves generated by the sudden release of strain energy (e.g., Khair, 1984; Lei et al., 2000; Rao et al., 1999). It is well established through experimental laboratory work with a variety of brittle materials, including rocks (e.g., Grosse and Ohtsu, 2008, Lockner, 1993), that AE rate increases proportionally with the formation and progressive

extension of both micro- and macrocracks. AE monitoring of rocks, or even concrete, under natural or simulated-natural, nonloaded conditions is significantly less common (Amitrano et al., 2012; Cohen et al., 2006; Girard et al., 2013; Hallet et al., 1991; Lyons and Austin, 2005). Because only cracking activity (collective crack growth), not mode (compressive vs. tensional fractures, for example), can be distinguished with numbers of AEs (Grosse and Ohtsu, 2008), throughout our work, we interpret numbers of

AEs as a proxy for overall cracking activity within the rock.

The chosen AE sensor employed herein was selected based on the high-frequency range, pre-amplification capabilities, and low power consumption necessary for this year-long field application (PK15I, manufactured by Physical Acoustics Corporation, Princeton Junction, New Jersey). In general, the magnitude or rate of crack growth that can be monitored with any given AE sensor depends on its frequency range (Grosse and Ohtsu, 2008). Because of their relatively high-frequency sensitivity (100–450 kHz), our sensors are known to detect emissions produced by both intermediate to fast subcritical rates of growth as well as critical coalescence of microfractures (Grosse and Ohtsu, 2008). By using a sensor with this operational frequency, extremely low magnitude and slow subcritical crack growth was not readily detected by our sensors. This exclusion was needed, however, in order to minimize the measurement of other low-frequency noise such as precipitation impacts. It is likely that our sensors measured such noise to some degree; however, we provide several lines of evidence that suggest that the majority of AEs presented herein were related to cracking (supplementary information DR1<sup>1</sup>).

Furthermore, in our study, if the elastic wave measurement received from a single AE sensor exceeded a predefined threshold value, data were recorded and referred to as an AE “hit.” If the same pulse was registered by at least four sensors on the boulder, it was regarded as an AE “event.” Our direct, real-time observations indicated that activity on or near the boulder (bugs crawling and/or landing on the rock, and people near the rock) sometimes produced AE hits, but such activity did not produce AE events (Warren et al., 2013). Additionally, dropping 2–3-mm-diameter drops onto the rock surface from 2.5 m height produced hits but not events. Nevertheless, because natural precipitation will have higher terminal velocity and thus more energy than laboratory-produced-drops, we cannot rule out that some measured AE events represent recorded precipitation impacts. Overall, however, we are cautiously confident that, by using moderately high-frequency sensors, and by observing “events” rather than “AE hits,” we were most commonly recording significant subcritical to critical crack growth activity in

the rock (supplementary information DR1 [see footnote 1]).

We employed a supporting software package (AE Win) capable of determining the three-dimensional location of AE events; for each event, an (*x*, *y*, *z*) coordinate was identified. The approximate accuracy of this location ( $\pm 25$  mm) was determined through a calibration process that involved determining the wave velocity field in the boulder; however, numerous AE events were found to be mislocated due to the natural heterogeneity of the boulder (Warren et al., 2013). Data presented herein have been filtered to only those AE events that fell within a +5 cm boundary of the rock.

### Measuring Surface Strain and Temperature

Surface strain (deformation) was monitored using Vishay Micro-Measurement rectangular rosettes (CEA-00-250UR-350; Fig. 1D). Given the ~5 mm maximum grain size of the boulder, each ~6-mm-long foil gauge spanned two or more individual mineral grains. In addition, standard, and widely used T-Type thermocouples (Omega SA1XL-T-120) were attached to the boulder adjacent to each strain gauge (Fig. 1C) at the following locations: the (1) top of the rock, (2) bottom of the rock, (3) north side equator, (4) east side equator, (5) south side equator, (6) west side equator, (7) midway above the equator in the northeast quadrant, and (8) midway below the equator in southwest quadrant. All locations were selected to document spatial variability while limiting the overall coverage of the rock with sensors and wires. There was no attempt to place sensors on particular minerals or in any particular orientation.

### Measuring Surface Moisture and Environmental Conditions

A Campbell Scientific 237F wetness sensing grid (Fig. 1) was attached to the top of the boulder to monitor surface moisture. Surface moisture data are bimodal (either “wet” or “dry”) based on a conservative threshold of resistance that was determined by a trial-and-error experiment with fine mist and individual drops of water. Any raindrops hitting another part of the boulder would not register “wet” in our data unless a drop had also hit the sensor.

In addition to the sensors that were installed on the boulder surface, to monitor the ambient environmental conditions experienced by the boulder, a weather station was installed adjacent to the rock, following standard meteorological setup protocols so that it could be readily compared with nearby weather stations. It measured ambient temperature and relative

humidity (CS215), wind speed and direction (CS03002), barometric pressure (CS106), insolation (CS300), precipitation (Texas Electronics TE525MM), and soil moisture (CS616).

### Field Deployment

The boulder was deployed in a pasture with full sun exposure near Charlotte, North Carolina (Fig. 1). The annual precipitation in the area averages 114 cm and is relatively uniform through the year. The mean annual temperature is 15 °C; average monthly temperatures range from 3.8 °C (January) to 26 °C (July), while average minimums and maximums range from –2 °C to 32 °C.

We compared the weather data from our field site for the time that the boulder was deployed with concurrent and long-term records from a nearby weather station (National Weather Service [NWS] Cooperative Observer [COOP] station number 313356, located ~6 km to SW of rock; Fig. 2) to determine whether the weather from the year of record was representative of the climate for the region. We first confirmed that there was a strong similarity ( $R^2 = 0.9$ ) between this weather station data and our own measurements. We then determined that compared to the 1951–1980 average monthly temperatures from COOP, monthly temperatures at the weather station near the rock were unusually cold from December 2010 to January 2011 (Fig. 2C). Other complete months were climatologically average months for the area. The sample period from July 2010 to April 2011 was drier (Fig. 2D) than average.

The site was selected due to a favorable combination of excellent sun exposure, security, and access. Additionally, the distance to the nearest road or power line was more than 1 km, which was important for minimizing background noise for AE monitoring. We tested for such background by sheltering the rock from direct sunlight and monitoring for AEs. During this relatively short, 1 h background monitoring period, no AEs were detected. In addition, we noted throughout the 11 mo record numerous sequential days with zero AE hits or events, including times with intense rainfall (Fig. DR1 [see footnote 1]). The boulder was set directly on bare soil, a red, sandy clay loam. A sturdy wire fence was constructed to keep cows or other large animals from interfering with the experiment. The boulder was oriented in the field in accordance with the north-south and east-west axes established during the sensor installation process.

### Data Acquisition and Analysis

AE activity was monitored by a Sensor Highway-II data acquisition system (Physical

<sup>1</sup>GSA Data Repository item 2016084, (1) a detailed analysis of the potential for recording precipitation impacts with our AE system, (2) thermal stress model parameters and (3) supplementary graphs of instrumentation data and/or modeling output, is available at <http://www.geosociety.org/pubs/ft2016.htm> or by request to [editing@geosociety.org](mailto:editing@geosociety.org).

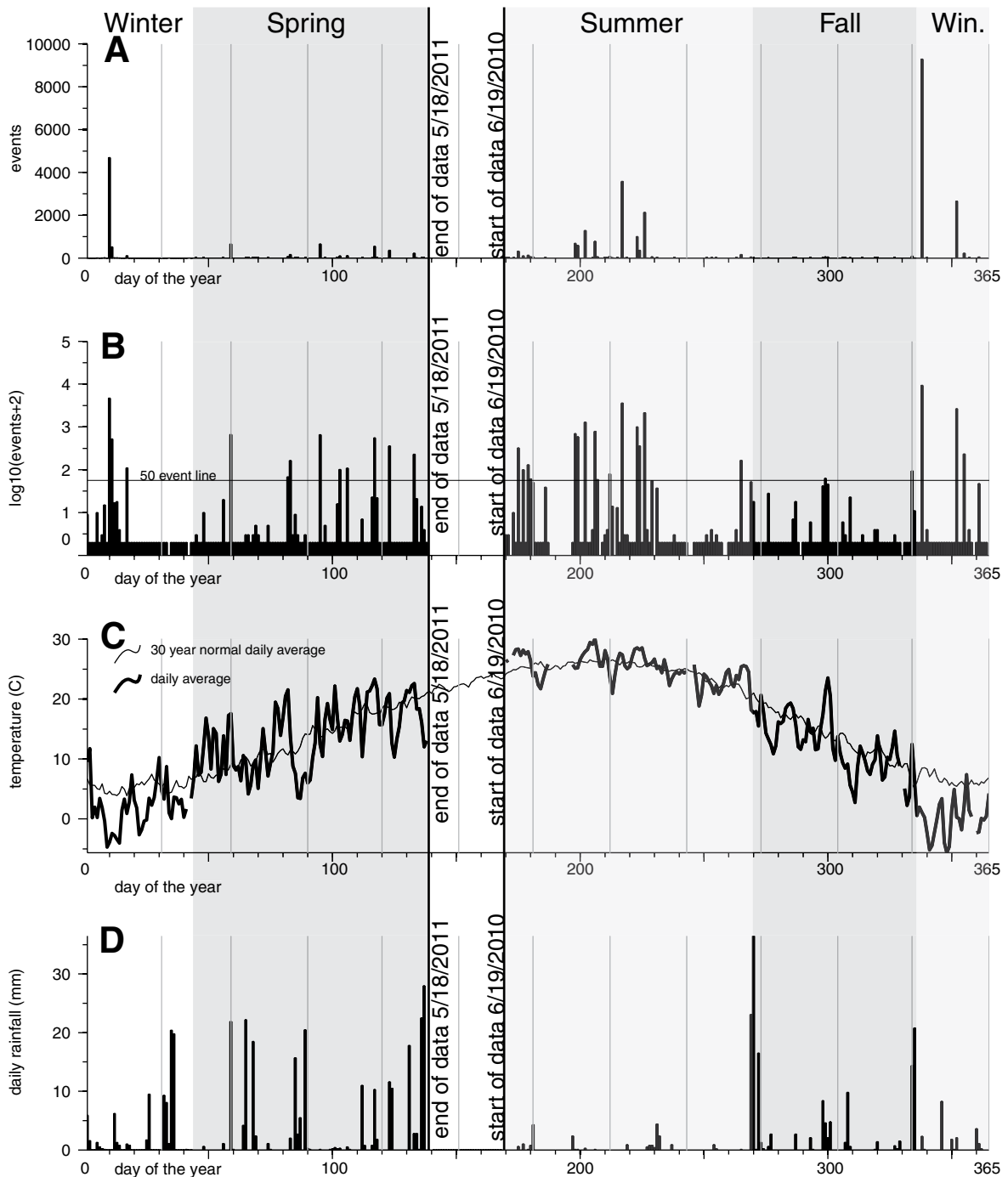


**Figure 2.** Time series for the entire monitoring period ordered by day of the year (1 = 1 January 2011; 360 = 31 December 2010). Any blank spaces represent times for which we were unable to collect data due to equipment malfunction. (A) Total numbers of daily events (total of 32,585 events). (B)  $\log_{10}$  (numbers of events +2) per day; depicting the data as  $\log_{10}(n + 2)$  allows visualization of the overall occurrence of events throughout the year with less emphasis on total numbers. 0 events plotted as 0.2. (C) Average daily temperature measured at the rock site (heavy black line) and average daily temperature derived from climate normal values (1951–1980; light black line) from a nearby National Weather Service (NWS) Cooperative Observer (COOP) station (see text). (D) Total daily precipitation measured at the rock site.

Acoustics Corporation). All other data were monitored and recorded by a Campbell Scientific CR1000 data logger. Time was recorded independently by both the CR1000 and the Physical Acoustics Corporation data logger. We recorded time offset and resynchronized these clocks every 2–3 d throughout the deployment period. The difference in time between the systems was typically less than 1 min.

Data were collected from 19 June 2010 to 18 May 2011. Occasional sensor and/or power malfunctions reduced the overall amount of data for any one sensor by varying amounts (e.g., lack of AE data seen in areas of Figs. 2A and 2B). In total, we collected AE data for 289 d, 9 h, and 36 min. All data are reported in local time, Eastern Standard Time.

### Brief Overview of a Prior Pilot Rock Deployment

Prior to this study, we conducted a 3 mo (June–August) deployment of a “pilot” rock of similar rock type with AE and surface temperature sensors installed exactly as in this study (hereafter

called “pilot deployment”; Garbini, 2009). We did not have surface moisture or strain data for the pilot deployment. In order to have easy and secure access to this first rock, it was deployed on the campus of the University of North Carolina at Charlotte, in a relatively sheltered and shaded location on the north side of a three-story building within 20 km of the field site described herein. Thus, it is useful to compare and contrast results from the pilot deployment (Fig. DR2 [see footnote 1]) to that of this study, as discussed in the results and discussion sections. For example, the sheltered boulder location of the pilot deployment provided a basis for considering the influence of shading on crack initiation and propagation, which is significant according to numerical modeling studies of thermal processes (Leask and Wilson, 2003; Molaro and Byrne, 2013).

## RESULTS

### Timing of Cracking

In total, 32,585 AE events were observed during the monitoring period. These events

were highly clustered in time; they occurred during 1201 individual minutes in 99 d (Fig. 2; Table 1). Hereafter “event times” and “event days” are individual minutes and days, respectively, in which events occurred.

The timing of events was strongly clustered at certain times of day (Fig. 3), with two primary clusters centering on 1:06 p.m. and 6:36 p.m., the latter of which corresponds with equinox sunset time for the latitude of the field site (6:20 p.m.). In total, 82% of all events occurred in two  $\pm 3$  h windows centered on these peak event times, with a tertiary peak occurring around midnight. In order to check that this finding was not due to sampling bias associated with disproportionately higher sensor functionality during those hours, we analyzed the total number of minutes of observation for each hour of the day throughout the recording period and found that all 24 individual hour-long periods were evenly monitored for all sensors in both studies.

For the pilot deployment, only 55 total events occurred during the 3 mo deployment period, 95% of which occurred shortly after sunset (~8:30 p.m.; Fig. DR2 [see footnote 1]).

TABLE 1. SUMMARY STATISTICS FOR ROCK SURFACE AND ENVIRONMENTAL CONDITIONS DURING ALL TIMES AND DURING AE EVENT TIMES ONLY

Measurement	Entire record	Event times only	$R^2$ measured vs. no. events	Pearson $r$ measured vs. no. events	Two-tailed Pearson $p$ value measured vs. no. events
<b>Environmental data</b>					
Avg. ambient temperature (°C)	13.4 ± 7.3	13.0 ± 5.6	0.003	-0.06	0.04
Avg. wind speed (m/s)	1.2	2.25 ± 1.9	0.003	-0.05	0.08
Avg. relative humidity (%)	70.9 ± 22.7	82.9 ± 14.8	0.000	-0.01	0.72
Total precipitation (mm)	504.8	41.3	0.001	-0.02	0.49
Avg. barometric pressure (mm Hg)	765.1 ± 4.6	763.7 ± 4.6	0.003	0.05	0.08
Avg. insolation (kW/m <sup>2</sup> )	0.18 ± 0.28	0.05 ± 0.10	0.008	-0.09	0.001
<b>Rock surface temperature</b>					
Avg. rock surface temperature (°C)	16.7 ± 12.8	16.0 ± 13.5	0.003	-0.05	0.08
Max. rock surface temperature (°C)	65.0	51.0	0.003	-0.05	0.08
Min. rock surface temperature (°C)	-15.1	-11.7	0.002	-0.04	0.17
Average daily surface temperature max – min (°C)	26.1 ± 8.3	22.2 ± 9.6	0.038	-0.19	0.06
Maximum daily surface temperature max – min (°C)	46.8	46.8	NA	NA	NA
Average within-minute (max – min) surface temperature (°C)	4.43 ± 3.44	3.07 ± 3.02	0.003	-0.05	0.08
Max. within-minute (max – min) surface temperature (°C)	23.6	16.09	NA	NA	NA
<b>Rock surface temperature change (°C) Calculated per minute</b>					
Avg. IDT/min	0.08 ± 0.04	0.14 ± 0.05	0.018	0.13	<0.001
Max. DT/min	15.5	2.1	0.006	-0.08	0.01
Min. DT/min	-14.2	-6.4	0.010	-0.11	<0.001
No. of minutes (events) recorded where  DT/min  > 2/min	3911	22 (902 events)	NA	NA	NA
No. of minutes (events) recorded where  DT/min  > 0.3/min	104,851	467 (14,900 events)	NA	NA	NA
<b>Calculated for a –5 min window</b>					
Avg.  ΔT/5 min	0.05 ± 0.08	0.1 ± 0.16	0.030	0.17	<0.001
Max.  ΔT/5 min	5.3	1.91	0.01	0.12	<0.001
<b>Calculated for a –10 min window</b>					
Avg.  ΔT/10 min	0.044 ± 0.05	0.083 ± 0.01	0.020	0.13	<0.001
Max.  ΔT/10 min	2.7	1.21	0.009	0.09	0.001
<b>Calculated for a –30 min window</b>					
No. of minutes (events) recorded where  ΔT/min  > 2/min > 10 times	6	2 (8 events)	NA	NA	NA
No. of minutes (events) recorded where  ΔT/min  > 0.3/min > 10 times	118,283	240 (3044 events)	NA	NA	NA

Note: Statistics were calculated for the entire record when event data were available ( $n = 416,680$  min) and again for only the minutes in which events occurred ( $n = 1201$  min or 99 d for calculations of daily data). Bivariate correlation statistics were calculated between the measured variable indicated in the far left column versus the number of events for each minute in which events occurred ( $n = 1201$ ). All temperatures are reported in °C. All rock surface temperature measurement calculations were based on all thermocouples for which data were available (typically eight each). Graphs of bivariate correlations are available in the supplementary information (Figs. DR1 and DR3–DR16 [see text footnote 1]). NA—not applicable.

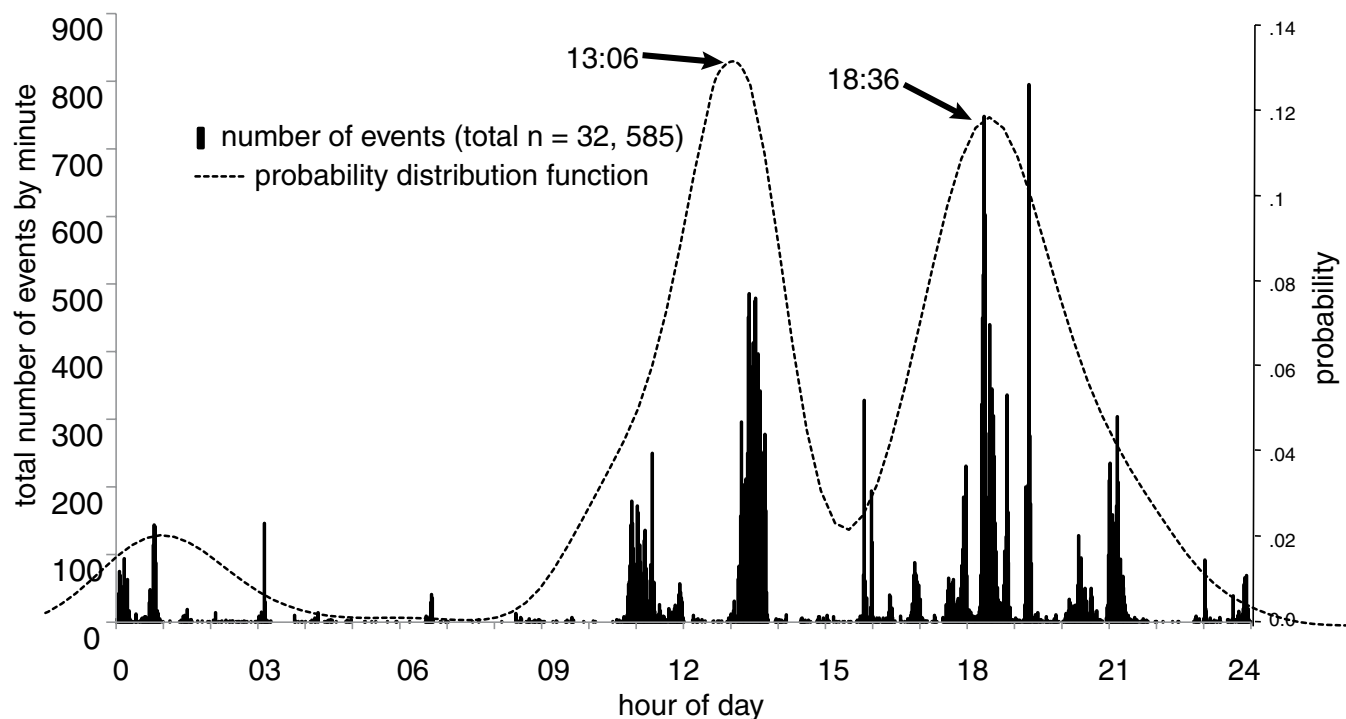


**Figure 3.** Histogram of the total number of events that occurred in each minute of the day for the entire period of record ( $n = 32,585$  total events). For example, there were 805 events that occurred between 8:18 and 8:19 p.m. (tallest bar on the graph). The dashed line is the calculated probability density function for the histogram.

To more fully describe the timing of event clusters recorded herein with respect to the diurnal cycle (i.e., did events occur before, during, or after sunset?), we examined data for the 34 event days that experienced 50 or more events (Fig. 4). These 34 “peak event days” represent 98% of the entire event population. Similar to the pilot deployment, most event clusters fell within 3 h after sunset on these peak event days, with a few occurring just prior to sunset when insolation dropped abruptly to near zero due to weather conditions (Fig. 4). Many event clusters also occurred around midday, roughly coincident with peak insolation. Most event clusters that fell outside of these times, such as early on 11 January, appeared to be continuations of event clusters that began the previous day (10 January, in this case).

### Cracking and Environmental Conditions

The vast majority of events occurred in clusters taking place during relatively short periods, 5 min to 1 h, during relatively few days (Figs. 2 and 4). Similarly, for the pilot deployment, the 55 events occurred during only seven clusters, each several minutes long (Fig. DR2 [see footnote 1]).

Such strong clustering is suggestive of specific factors triggering cracking; however,

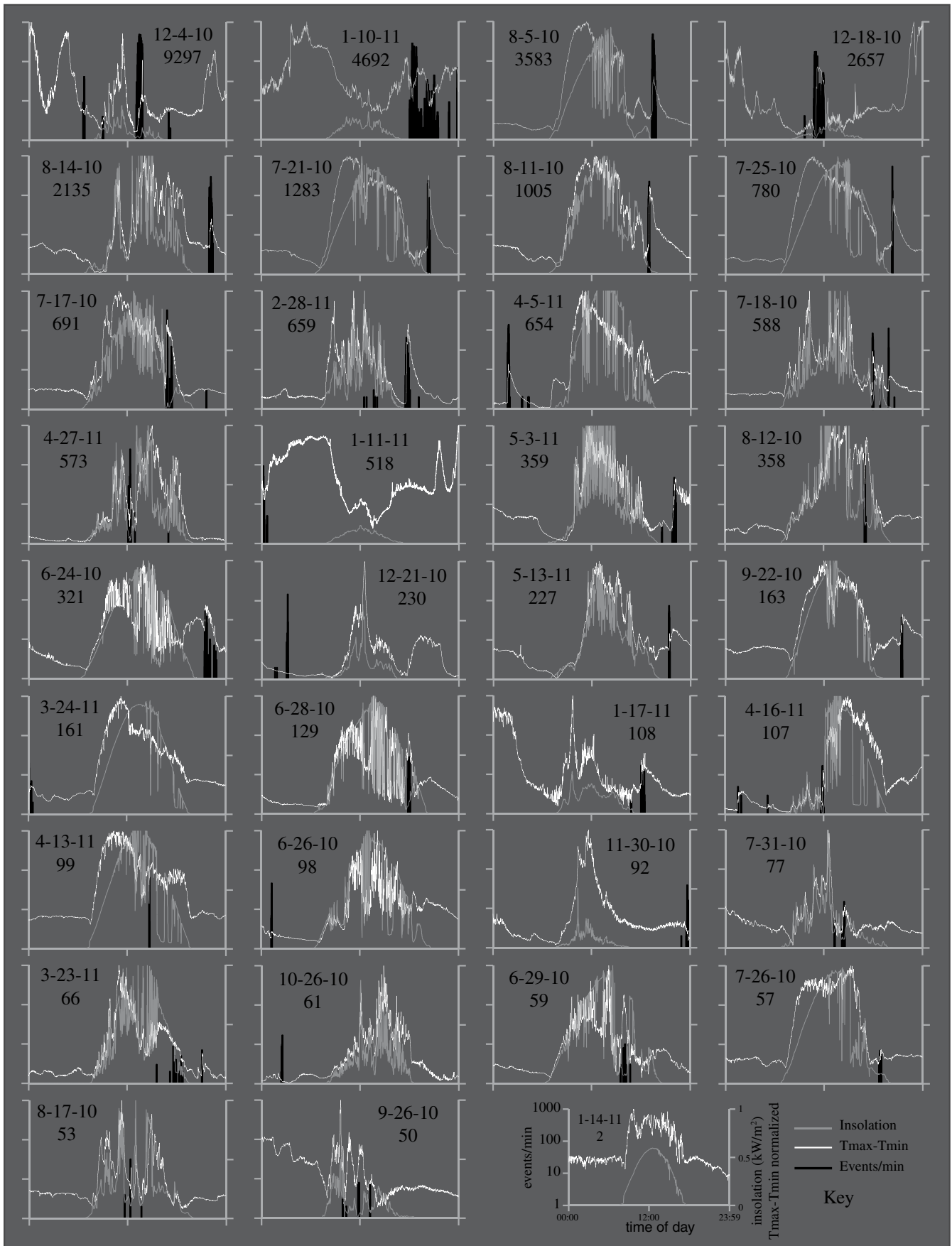
there were no statistically robust bivariate correlations between observed AE event rate and environmental characteristics or measured rock surface temperatures for event times (Table 1; Figs. DR1 and DR3–DR16 [see footnote 1]), nor were there clear trends when AE energy was considered and potential sampling biases were evaluated (Figs. DR17 and DR18 [see footnote 1]). For example, events did not typically occur during the early morning hours when the rock was most often wet, likely due to dew (Fig. 5), or during the overnight and morning hours, when it was most often experiencing freezing temperatures (Figs. DR3 and DR11 [see footnote 1]). Furthermore, extremes measured over the entire period of record in any given environmental or rock surface condition were typically larger than those occurring coincident with periods of crack growth (Table 1; Fig. 6).

We therefore further examined the environmental and rock surface data for the same 34 high-event days recorded in the data set to determine if qualitative trends or correlations could be observed in daily data. In 33 of these days, the primary event cluster coincided with a relatively rapid and distinct cooling or heating of some portion of the rock surface relative to other parts (white lines in Fig. 4 show the total surface temperature range). All of these instances appeared

to be driven by an abrupt change in weather (see following). As with the rock described herein, 98% of all events recorded in the pilot study also coincided with a relatively rapid change in surface temperatures (red lines in Fig. DR2 [see footnote 1]) that was hypothesized to be linked to dynamic weather (Garbini, 2009).

Based on our 1 min averages, the rate of change of rock surface temperature during all event times was almost twice that of the overall period of record (Table 1). In many instances when the range of rock surface temperatures was changing rapidly at times of day other than midday and sunset, however, no events occurred (e.g., Fig. 4, 8/5/2010, 12/4/2010, 1/10/2011). The only high-event day when events did not coincide with notable surface temperature change, 21 December 2010, encompassed 230 events (Fig. 4); we attribute these events to ice growth (see subsequent section).

The abrupt rock surface heating and/or cooling that often coincided with events did not generally result in extreme temperature differences across the rock surface (i.e.,  $T_{\max} - T_{\min}$  during any given minute); this difference during event minutes averaged only  $\sim 3$  °C, whereas the maximum difference over the period of record was 23.6 °C (Table 1). The geometry and gradient of the surface



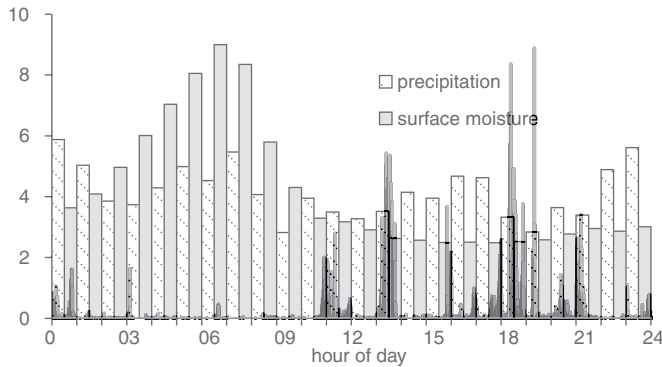


**Figure 5.** Histogram organized by hour of the day for the entire period of record depicting total instances any rainfall measured on site during that time of day and total instances of the rock surface moisture sensor registering “wet” during that time of day. The event histogram from Figure 3 is superimposed in the background of the graph.

observed rock surface temperatures, weather changes, and AE events, we present details of the 5 d during which the highest numbers of events occurred, which encompass ~70% of all events. These 5 d account for less than 1.5% of the period of monitoring (Figs. 8–10). With a few noted exceptions, these high-event days illustrate the links that are consistent throughout the entire data set among weather changes, rock surface temperatures, time of day, and cracking.

**4 December 2010—9245 AE events.** Almost 30% of all events occurred on 4 December 2010 (Fig. 8). This day marked the first continuously cold day of the 2010 winter. Despite its record number of events, this event day is representative of high-event days that occurred during colder weather. Namely, it occurred around midday and overall coincident with abrupt surface temperature variation driven by the onset of a frontal rain system, which is visible on this day as a dramatic increase in relative humidity (Fig. 8A).

The main event cluster, which constituted 98% of the events for the day, occurred within a single hour, 1:02–1:47 p.m. (Fig. 8B). The surface of the rock had been cooling steadily, likely due to the decreasing air temperature associated with the approaching weather system (Fig. 8A). Shortly before events began, however, insolation started increasing, and westerly winds

temperature field during event times reflect this result (Fig. 7); it is similar in shape and orientation to the temperature field averaged over the entire period of record, but the contrast between the hottest part of the rock and the coolest during events is smaller.

The direction of temperature change (heating vs. cooling) of the rock surface was not consistent during event times. During the entire period of record, 7882 events (out of 32,585) transpired when all eight thermocouples were cooling, and 453 when they were all warming. Thus, during

the remaining more than two thirds of event times, rock surface temperature changes were spatially complex, with parts of the rock cooling while other parts were warming.

**Detailed Look at the Five Highest-Event Days**

In order to further illustrate the details of the complexities and repeating relationships among



**Figure 4.** Daily time series (1440 min) of data for the 34 d during the period of record that experienced 50 or more events in the day (ordered by decreasing numbers of total events); 98% of all events occurred during these days. The date and total number of events for the day are depicted on each graph. The left y axis is a log-scale of event rate from 0 to 1000 (top tic) events/min. The right axis is both raw insolation data (kW/m<sup>2</sup>, grey color) and the difference between the temperature of the hottest and coldest thermocouples in each minute, normalized by the daily maximum difference (white color). Normalization allows for comparisons between all 34 d using the same scale. The key depicts a typical relatively cloudless and windless day in the period of record with very few events. This date’s data were used for validation of the numerical model presented in the discussion portion of the text.

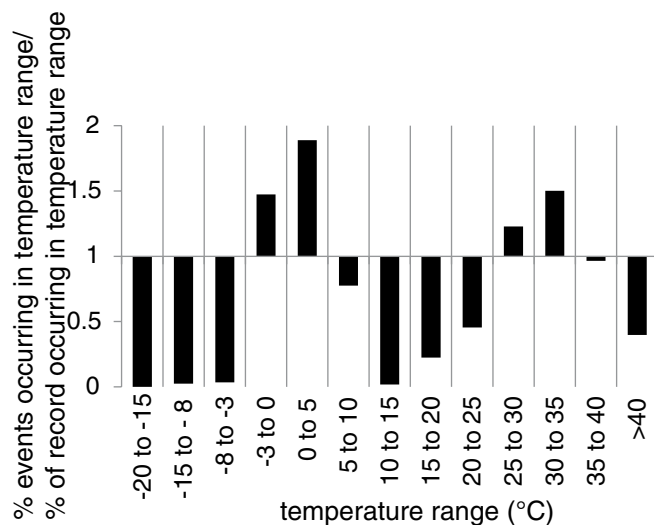


**Figure 6.** This graph depicts the proportion of all events (total  $n = 32,585$ ) occurring when the rock surface experienced specific surface temperature ranges divided by the overall proportion of minutes (total  $n = 416,680$ ) that some portion of the rock surface was within that range. As such, values close to unity would be expected if events were occurring completely randomly in the context of rock surface temperature; values  $>1$  indicate that events preferentially occurred in those certain temperature categories; and values  $<1$  indicate that fewer than expected events occurred in that temperature range.

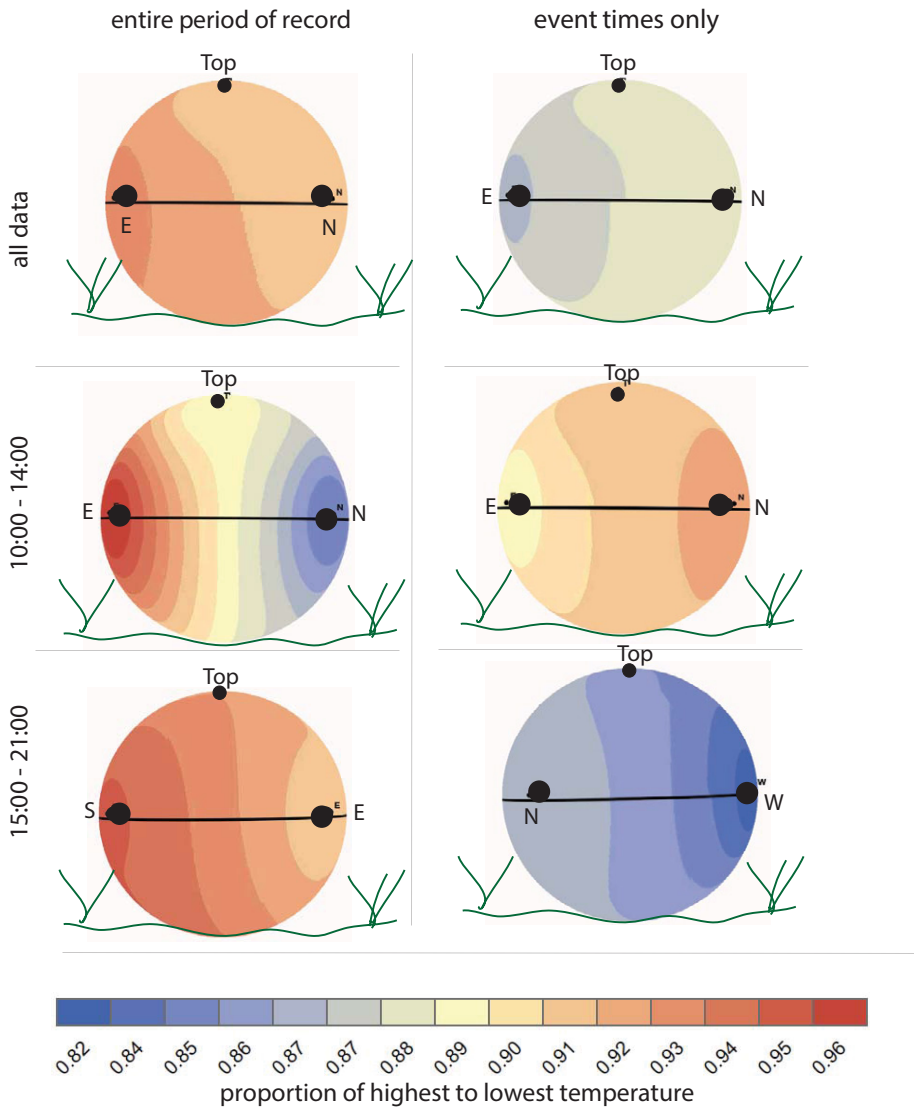


**Figure 7.** Depiction of the measured temperature field of the boulder at different times of day. Temperatures between thermocouples were calculated based on inverse distance interpolations to create a continuous surface of rock temperatures. As such, overall isotherm geometry as well as temperature gradients from highest to lowest can be compared for event times and for the entire period of record. Colors represent the average deviation of surface temperature in any given location from maximum surface temperatures at the same time of measurement. As such, the larger the color contrast, the higher is the relative magnitude of difference in temperature across the rock surface at the times depicted. Note that in each depiction, only a little over a quarter of the circumference of the sphere is visible due to inherent distortion that results from plotting three-dimensional data in two dimensions. The portion of the boulder with the greatest calculated contrast is depicted, and so the view is different for the third row of data. Boundaries between colors depict the orientation of isotherms on the boulder surface. Surface temperatures ( $T$ ) were first normalized by the maximum value (between the eight thermocouples) during each minute  $i$  ( $T_i/[\max T_1 \text{ to } T_8]$ ), giving a number between 0 and 1 for each thermocouple for each minute, where the hottest thermocouple of each minute would have a value of 1. These normalized values were then averaged for the entire period of record as well as for certain times of day (left column). Then, for times in which events occurred (right column), a weighted average was calculated for the latter by weighting each minute's value by the number of events that occurred in that minute.

slowed (Figs. 8B and 8C, arrow 1). As a result, the top and west thermocouples began warming, while cooling slowed in other locations on the rock surface (Figs. 8B and 8C, circle 1). Similar reversals in cooling or warming that were coincident with event onset/intensification were common in most high-event days, and these reversals are reflected in increasing or decreasing differences in temperature across the rock surface visible in Figure 4.

Also as with most other high-event days, the onset of the event cluster essentially coincided with the onset of moisture on the rock surface. In this case, moisture was detected 3 min (Figs. 8B and 8C, indicated by blue background) after events began. Rain was not sufficient to trigger the 0.1 mm tipping bucket until 21 min later (arrow 2), but hourly observations from a nearby weather station indicated heavy fog and mist during this time, which likely resulted in wetting of the rock surface.

Shortly after moisture was registered by the moisture sensor, all surface temperatures started to decrease. By 1:08 p.m., winds picked up, and surface temperature on the top of the rock markedly dropped ( $\sim 0.5$  °C in  $\sim 10$  min), followed by other locations (Figs. 8B and 8C, circle 2). During this time, the event rate increased from dozens/min to almost 300/min. This type of abrupt surface cooling in the presence of wind and moisture was also common during event clusters on other high-event days. The cooling likely arose from both higher heat advection and evaporative cooling.

**10 January 2011—4692 AE events.** The second highest number of events on a single day occurred on 10 January 2011 (Fig. 9), during a rare snow and freezing-temperature day in the Charlotte region. In the period leading up to the event cluster, air temperatures had remained below freezing since  $\sim 5$  p.m. the previous day, and it started to snow around 4 a.m. of the event day (Fig. 9A). Just prior to the onset of this snow, a rapid drop in air temperatures resulted in an almost 1 °C cooling of the rock's top surface relative to its base within a few minutes (Figs. 4 and 9A). Only a single event occurred shortly after this time of relatively rapid and extreme weather change, highlighting that events transpired much less frequently during abrupt onset of weather and associated temperature change when such changes occurred during late-night and morning hours than during the middle and end of the day (Fig. 4; see following section, which more fully explores this idea).

The primary event cluster of the 10 January day occurred around 6:00 p.m. and roughly coincided with a switch from ice pellets to freezing rain (liquid precipitation that freezes on contact with the ground surface), as indicated

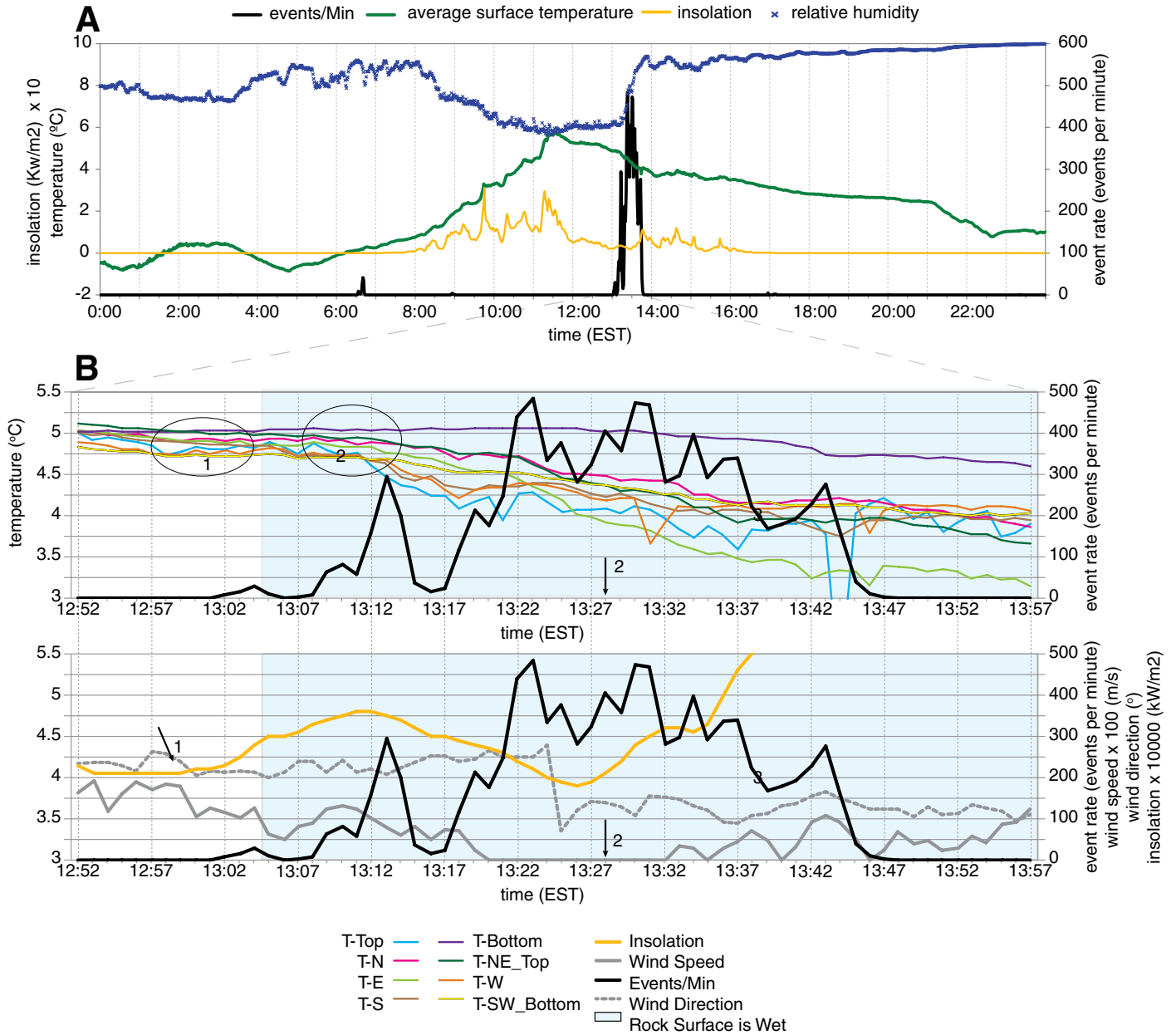


**Figure 8.** Time series of various data for 4 December 2010. (A) Midnight to 11:59 p.m. (B) The period of the primary event cluster of the day depicting rock surface conditions. (C) Same period as B depicting various environmental conditions. See text for explanation of arrows and circles. EST—Eastern Standard Time, T-Top—top thermocouple, T-N—north thermocouple, etc.

by hourly observations of precipitation from a nearby local weather station (Fig. 9A). There was a period of rock surface warming at this time, the onset of which preceded the event cluster by ~15 min and occurred about an hour after sunset (Fig. 9B). The warming of the surface of the rock was particularly abrupt on the top, east, and south sides of the rock, where temperatures rose ~0.4 °C, 0.6 °C, and 1.3 °C, respectively, in ~15 min (Figs. 9B and 9C, circle 1), presumably due to the release of latent heat upon freez-

ing associated with the onset of freezing rain. The bottom of the rock as well as the north side (possibly under snow, since winds were from the north) showed little change in temperature during this time. Event rate increased significantly when the top thermocouple began to heat up again (arrow 1), and a second peak in event rate occurred shortly after the south side of the rock experienced significant cooling, likely in response to an increase in wind speed (circle 2). Hourly weather data indicated that freezing

rain continued on and off for the remainder of the day (Fig. 9A); subsequently, similar surface warming and smaller event clusters continued into the early morning hours of 11 January (Fig. 4).

**5 and 14 August, and 18 December 2010.**

Three additional highest-event days illustrate a pattern representative of the majority of days with events (Fig. 10). The onset of event clusters tended to coincide with periods of relatively accelerated heating or cooling of some portion

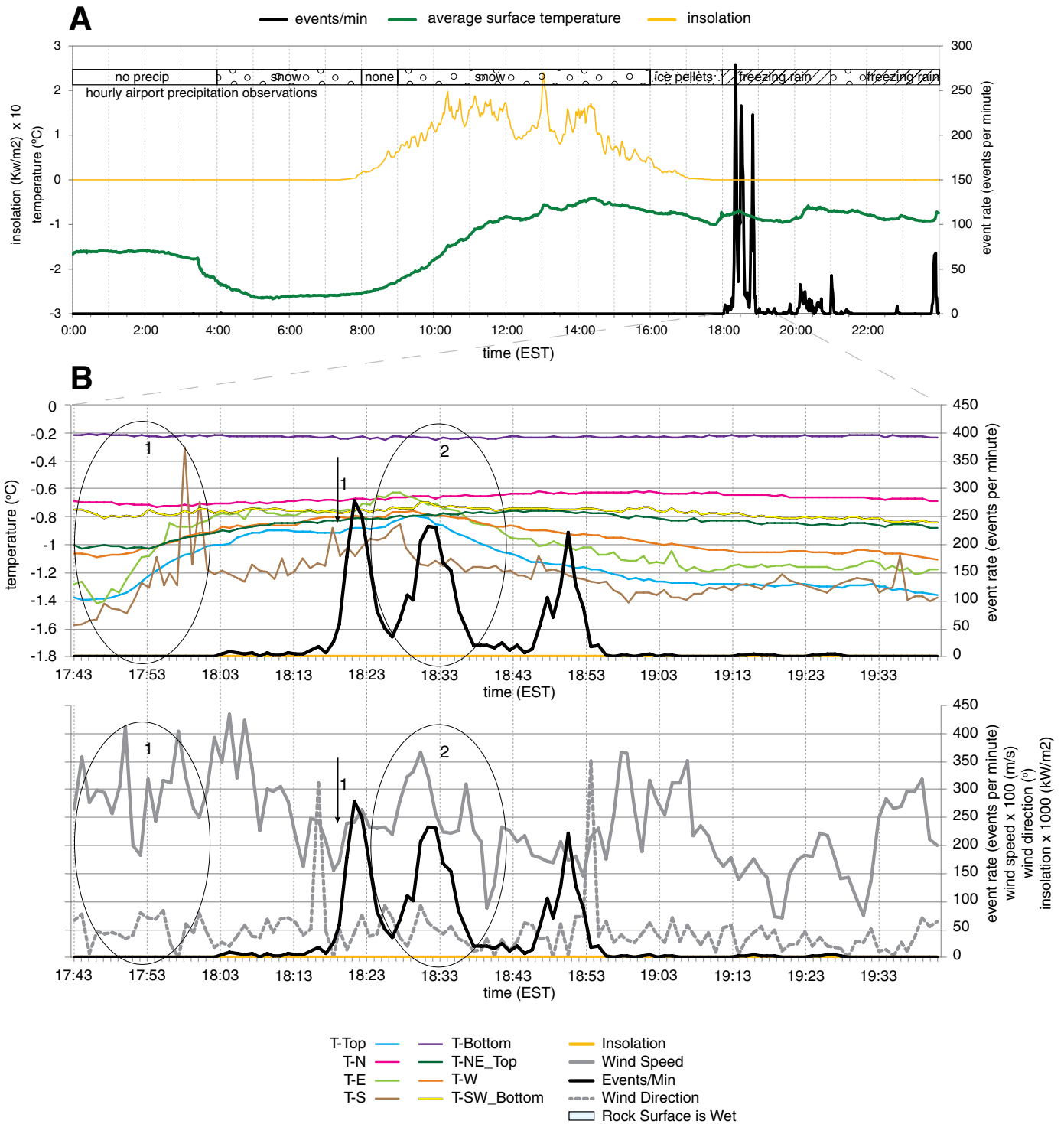


**Figure 9.** Time series of various data from the weather station adjacent to the rock or the rock surface for 10 January 2011. (A) Hourly precipitation data are from KAKH Gastonia Airport ASOS station (35.2026594°N, 81.1498675°W) for 24 h starting at midnight. (B) Period of the primary event cluster of the day depicting surface temperatures. (C) Same period as B depicting various environmental conditions. See text for explanation of arrows and circles. EST—Eastern Standard Time, T-Top—top thermocouple, T-N—north thermocouple, etc.

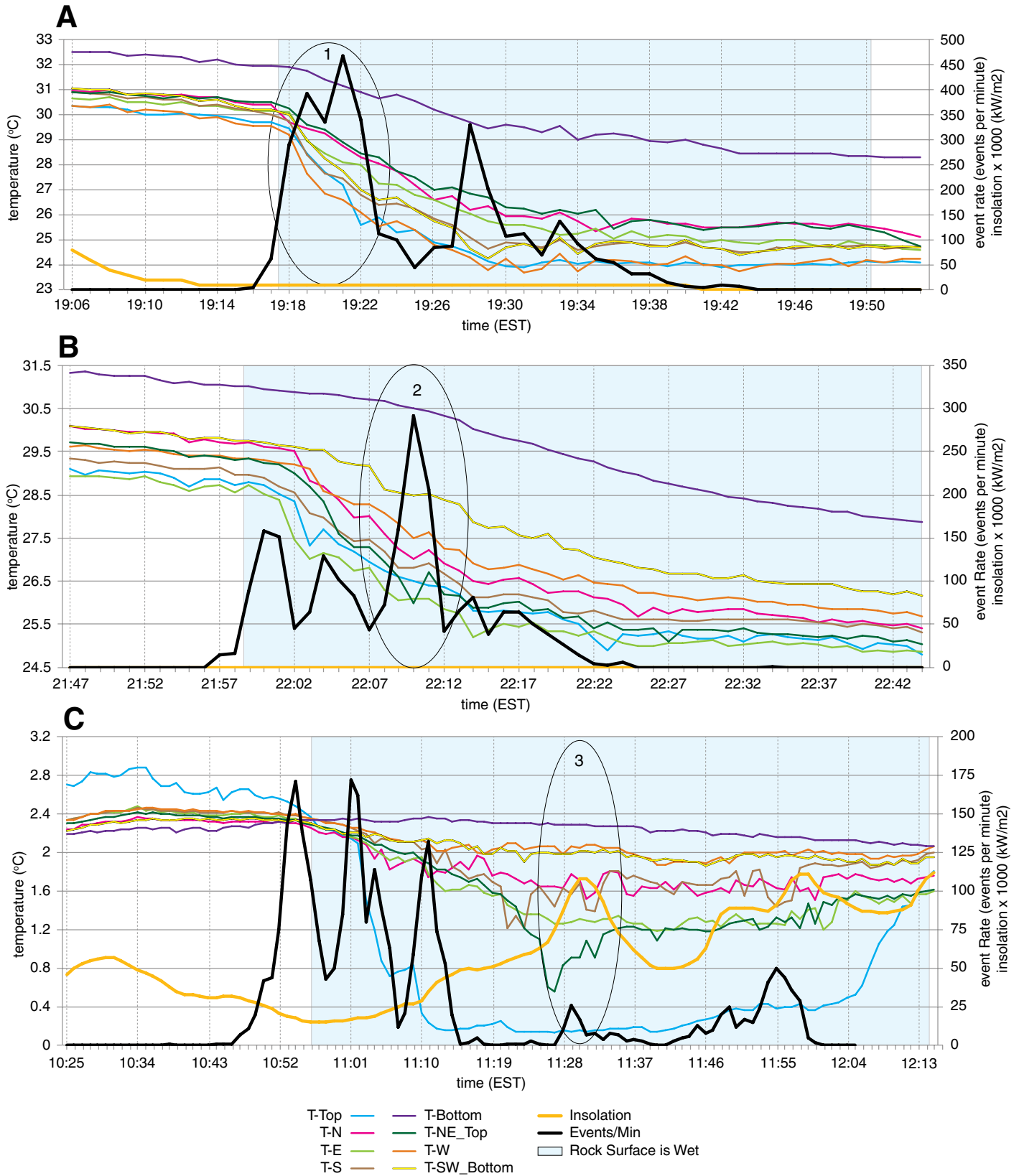


**Figure 10.** Time series of various data for the primary event cluster occurring on (A) 5 August 2010, (B) 14 August 2010, and (C) 18 December 2010. See text for explanation of circles. EST—Eastern Standard Time, T-Top—top thermocouple, T-N—north thermocouple, etc.

of the rock surface relative to the remainder of the rock. Subsequent increases in event rate on virtually all high-event days, including the three depicted in Figure 10, typically coincided with accelerations (e.g. Fig. 10A, circle 1), decelerations, and/or reversals (e.g. Fig. 10B, circle 2; Fig. 10C, circle 3) in surface temperature change that could be linked to dynamic environmental conditions. On all three of these days, the primary event cluster coincided with the onset of a weather event.

### Rock Surface Strain

Strain data presented herein provide direct evidence of expansion and contraction of the monitored boulder surface (Fig. 11). The strain data indicate that the rock surface responded measurably to temperature. On most days, the principal strain (a calculation derived from all three gauges in a single rosette; Fig. 1D; Warren et al., 2013) for all strain rosettes followed similar, although somewhat smoother trends than those of surface temperature. When the boulder surface warmed and cooled, the maximum principal strain on the surface rose and fell, respectively (Fig. 11A). Hence, the data set reveals regular, cyclic elastic surface expansion and contraction of the boulder due to diurnal temperature variations. The average daily fluctuation in maximum principal strain was on the order of hundreds of microstrain, equivalent to roughly  $\sim 3 \mu\text{m}$  of length change of the 6 mm foil. However, such quantifications should be viewed in light of the errors associated with the inherent complexities of calculating strains on a polycrystalline, uneven rock surface (Warren et al., 2013).

Over the short time intervals when event clusters occurred, an accompanying relatively abrupt dip or rise in strain often corresponded with the overall abrupt cooling or warming (arrow in Fig. 11A). These strain anomalies scaled with temperature; the changes in maximum principal strain were typically  $\sim 50\text{--}100 \mu\text{strain}$ . However, similar drops (and jumps) commonly occurred during times when temperatures were rapidly changing, and no events transpired. Thus, although strain measurements provide insights into the deformation at the rock surface in the context of temperature change, the relationship of such deformation and the state of stress in the rock appears to be complex. Hence, large surface deformation does not necessarily coincide with cracking activity, at least not at energies sufficient to generate events recorded by our AE sensors.

In addition to diurnal cycles of relatively elastic strain, during the course of the experiment, we recorded permanent positive strain, net extension, on all gauges except the gauge on the

bottom of the rock, which showed virtually no change (Fig. 11B). The top, west, and southern gauges recorded the largest net extension over the course of the study, while the east and north sides showed the least. This net residual expansion of the boulder is consistent with our interpretation of AE data as fracture activity, because it likely reflects the relative increase in the collective volume of cracks, new and old, during the experiment.

Acceleration in measured strain accumulation seldom coincided with acceleration in event rate; however, there was a stronger coincidence between accumulated strain and accumulated hits (Fig. 11B). Thus, similar to other AE cracking studies (e.g. Beattie, 2013), strain (and hit) accumulation during times without AE events in this study might be reflecting controlled, time-dependent subcritical crack growth that occurs at rates and energies too insufficient to produce events, but sufficient to record hits, and in some cases neither. With the exception of the western gauge, surface strain did not increase at rapid rates during winter months when freeze-thaw might be most active in the rock, nor did the location of the highest amounts of accumulated strain always correspond to measured locations of the majority of AE events (see following section).

Caution is needed in interpreting these long-term strain records because of inherent difficulties with prolonged field-based strain experiments; creep-like deformation can arise with time due to aging components of the experiment, including the electronics, the gauges, and the gauge-rock coupling (adhesive). We did not, however, observe any visual evidence of such deterioration of any of our sensors at the end of the deployment. Results from future deployments will help to determine the extent to which strain measurements are reflective of inherent rock deformation patterns.

### Cracking Locations

Measured AE events were primarily located in the upper hemisphere of the boulder; very few events were located in the lower hemisphere (Fig. 12A). Accurate pencil lead-break tests on the bottom of the rock showed that this preferred localization was not related to sensor location (Warren et al., 2013). Furthermore, similar clustering was observed in the upper hemisphere during the pilot test deployment of the boulder in North Carolina (41 of 55 events were in the upper hemisphere; Garbini, 2009), and the strain gauge placed in this study's rock upper hemisphere experienced the highest, by a large margin, net expansion over the monitoring period (Fig. 11B).

Calculations of the distance of AE event locations measured in all directions from the center of the rock further revealed that a majority of events fell in one of two locations with respect to the rock surface: either right at the surface of the boulder (spanning the right-hand peak in Fig. 12B), or in its interior  $\sim 6\text{--}10 \text{ cm}$  from the surface. The nonsphericity of the rock surface likely dictated the geometry of the tails of these peaks. There was not, however, a time-of-day preference for these interior versus exterior locations (Fig. 12C), despite the modeling prediction that one might exist (see Discussion).

Overall, measured cracking locations were preferentially concentrated in the northern and eastern portions of the rock (Figs. DR19 and DR20 [see footnote 1]). With few exceptions, notably 10 and 11 January (see Discussion), these locations are similar when high-event days are considered individually, including the one high-event day that was not associated with rapid temperature changes and that we attribute to ice growth (21 December; Fig. DR20 [see footnote 1]). These data provide evidence of consistency in cracking location through time.

Locations of events measured herein differ from the western concentration of events measured in the pilot deployment (Garbini, 2009), as well as from areas of relatively high permanent strain in this study (west- and south-facing sides of the boulder; Fig. 11). It is possible that accumulated strain in the western portions of our boulder did not result in cracking detected by our AE sensors. Also, however, the locations of known events in this region of the rock revealed unusually poor precision during calibration tests, likely due to the effects of differences in concentration of preexisting cracks on wave velocities in the area around the western "dimple" (Warren et al., 2013). Also, almost 60% of all measured AE events were not located within the boulder envelope itself (Warren et al., 2013), a common issue of localizing AE in heterogeneous material (e.g., Grosse and Ohtsu, 2008); thus, the location data presented reflect less than half of the cracking activity.

In addition to the locations of AEs, we observed the formation and/or expansion of several visible cracks on the surface of the rock over the course of the 11 mo deployment (Figs. DR19–DR22 [see footnote 1]). Prior to deployment, with the exception of the region around the "dimple" found on the western side of the rock (Figs. DR21 and DR22 [see footnote 1]), there was no significant evidence of separated cracks on the boulder surface (Figs. DR23A and DR24A [see footnote 1]). After deployment, in several locations on the surface, particularly along irregular edges of

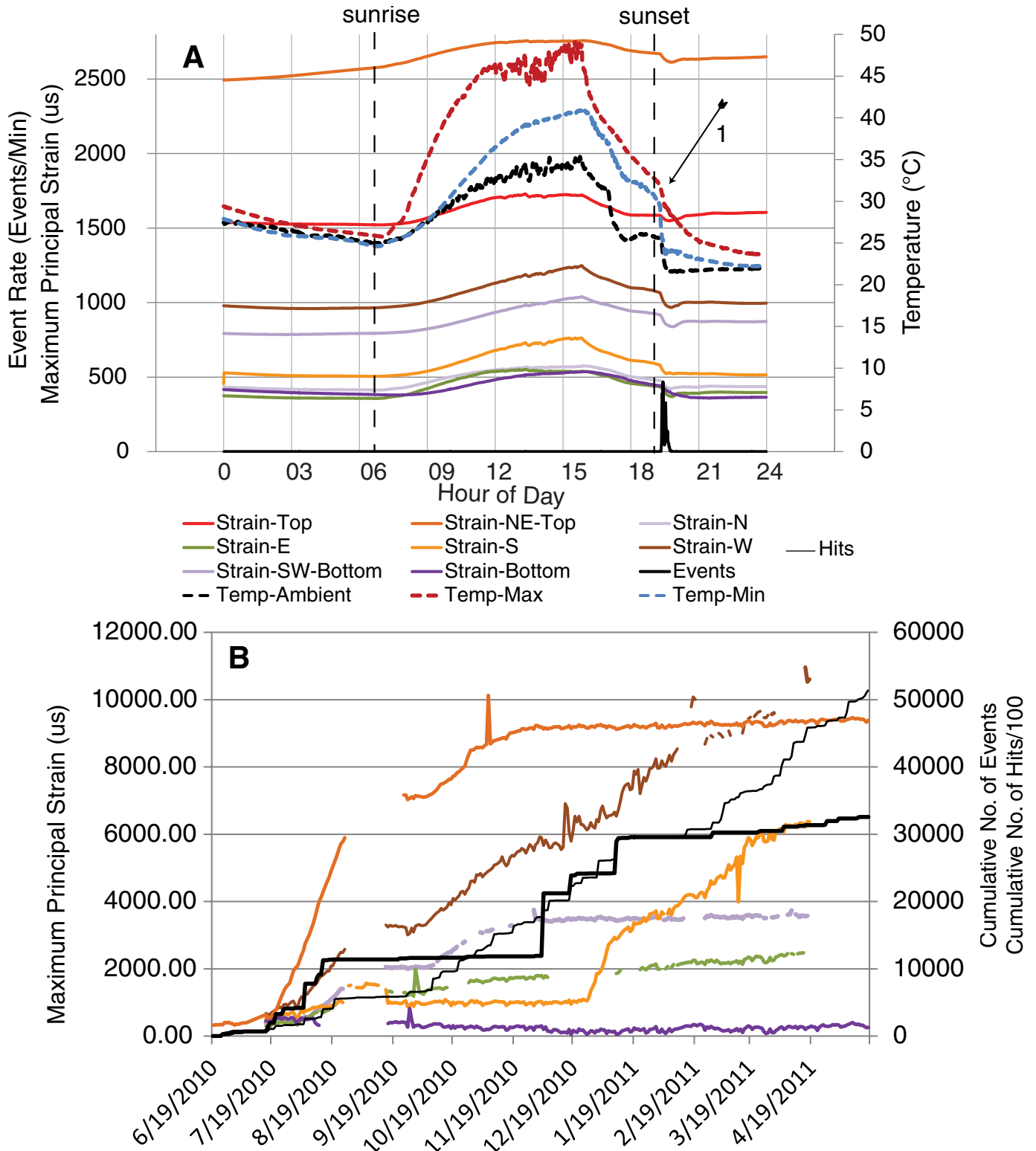
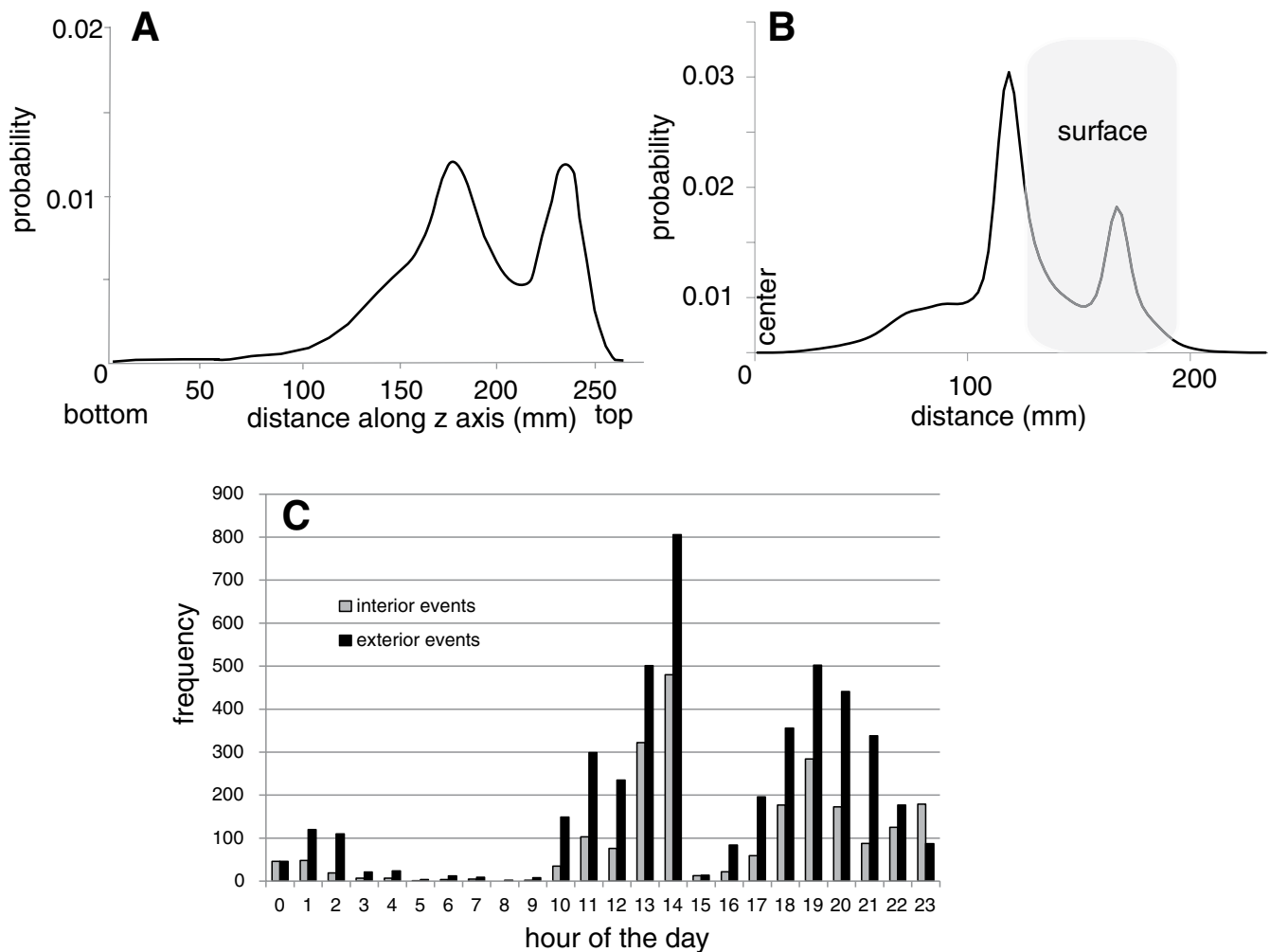


Figure 11. Maximum principal strain calculated for surface strain gauges plotted with events. (A) Strain measured on a single day (5 August 2010; depicted in Fig. 10A) plotted with ambient temperatures, maximum and minimum temperatures measured on the rock surface, and event rate (events per minute). (B) Daily average of maximum principal strain for surface strain gauges plotted with the cumulative sum of all acoustic emission (AE) events (heavy black line) and AE hits (thin black line). Note that the offset in strain between different sensors in A represents the differences in accumulated strain over the course of the deployment seen in B. All sensors were calibrated prior to deployment to a strain of zero (Warren et al., 2013).



**Figure 12. Acoustic emission (AE) localization data for AE events. (A) Probability density function of the localization of events along the rock's vertical  $z$  axis only. 0 is the bottom of the rock. (B) Probability density function of the distance of localized events from the center of the rock regardless of direction. 0 is the center of the rock. The shaded area encompasses the minimum and maximum rock radius. Note two peaks, one just at the rock surface, and the other ~6–10 cm from the surface toward the interior of the rock. The nonsphericity of the rock surface is likely dictating the geometry of the tails of these peaks. (C) Distribution of the timing of events for all events occurring within  $\pm 10$  cm of the two different peaks (interior vs. exterior) depicted in B.**

protruding grains, we found prominent open cracks (Figs. DR23B, DR24B, and DR22 [see footnote 1]), as well as evidence of the removal of individual mineral grains (e.g., the region around the dimple showed evidence of active granular disintegration [loose crystals easily rubbed off] after deployment [Fig. DR22 circle, see footnote 1], and one mafic mineral in the lower left of circle in Figure DR23 [see footnote 1] appeared to be missing).

The locations (north and east side of the boulder) of these newly formed, or further opened, visible macrofractures generally correspond to locations of AE events (dominant in the northern and eastern quadrants of the boulder; Fig. DR19A [see footnote 1]), on most days (e.g., Fig. DR20 [see footnote 1]). As previously

mentioned, AE events were not commonly located on the western side of the boulder, which exhibited significant evidence of postdeployment macrofracture, but accumulated strain was particularly high on that side. A full spatio-temporal analysis and three-dimensional (3-D) visualization of AE event locations is beyond the scope of this paper but may provide insights into these observations.

#### Timing of Intense Weather versus Events

In order to more clearly document the extent to which severe weather in and of itself might be correlated with AE events, we examined a relatively small population of weather extremes: instances with rainfall intensities

$\geq 0.3$  mm/min. Given the 0.1 mm capacity of our tipping bucket, this rate indicates a minimum rainfall intensity equivalent to 12 mm/h within the minute for which the rate was recorded. Throughout the entire record, rainfall intensity reached 0.3 mm/min or greater during 188 individual minutes on 24 different days. In total, 808 events occurred during 40 of those minutes (Fig. 13), and 97% of these 808 events transpired within a few minutes of the onset of the intense rainfall, continued for a few minutes to an hour or two, and then event rate decreased, even when rain intensity became high again (e.g., Fig. DR25 [see footnote 1]).

For all instances when intense rain commenced with no prior rainfall in the noon-to-midnight hours, at least some events were

recorded. Conversely, when intense rainfall started earlier in the day, and/or persisted into afternoon hours, it was not always or often coincident with events. For example, during the 68 different minutes in which rainfall intensities were  $\geq 0.3$  mm/min between midnight and noon, only 14 events occurred during 3 event minutes (Fig. 13). Even when such rainfall resulted in temperature drops on the order of 4 °C over 30 min, events were not typically measured if the rainfall occurred in the morning hours. Thus, this analysis, combined with our previous observations, suggests that weather such as wind or rain possibly drives cracking only when it induces a significant change in surface temperature, and generally only if that change occurs during afternoon and evening hours.

## DISCUSSION

### Numerical Modeling of Solar-Induced Thermal Stresses

In order to obtain a quantitative understanding of macroscopic stresses associated with simple solar forcing of our study boulder, Shi (2011) developed a thermo-mechanical model of the thermal and stress states in idealized boulders sitting on the ground in open sun (Hallet et al., 2012). Using commercial

finite element software (MSC.Marc2008r1), the model calculates the 3-D thermal evolution of boulders resulting from radiation and conduction for idealized diurnal variations in solar radiation. The sun is treated as a perfect black body, with emissivity of 1 and constant temperature of 5778 K. The net energy flux into the boulder is computed from the sum of the coupled influxes due to solar radiation directly from the sun and from the ground surface, as well as heat exchange with the soil and sky, represented here simply as having a fixed temperature of 253 K (−20 °C; A. Gillespie, 2011, personal commun.). Using the calculated temperature field over a diurnal cycle, and treating the boulder as a homogeneous, isotropic, linear elastic solid, the model then calculates the thermally induced stress field over that same diurnal cycle. Representative thermal and elastic parameters are used for rock and soil (Table DR2 [see footnote 1]).

The temperature component of the model was validated by running the model for a boulder resembling the instrumented boulder described herein in terms of size, shape, and material properties appropriate for rock and soil, date and location (latitude). The comparison between the measured and modeled surface temperatures during a representative cloudless winter and relatively still day (14 January 2011; key of Fig. 4) shows that the model reproduces

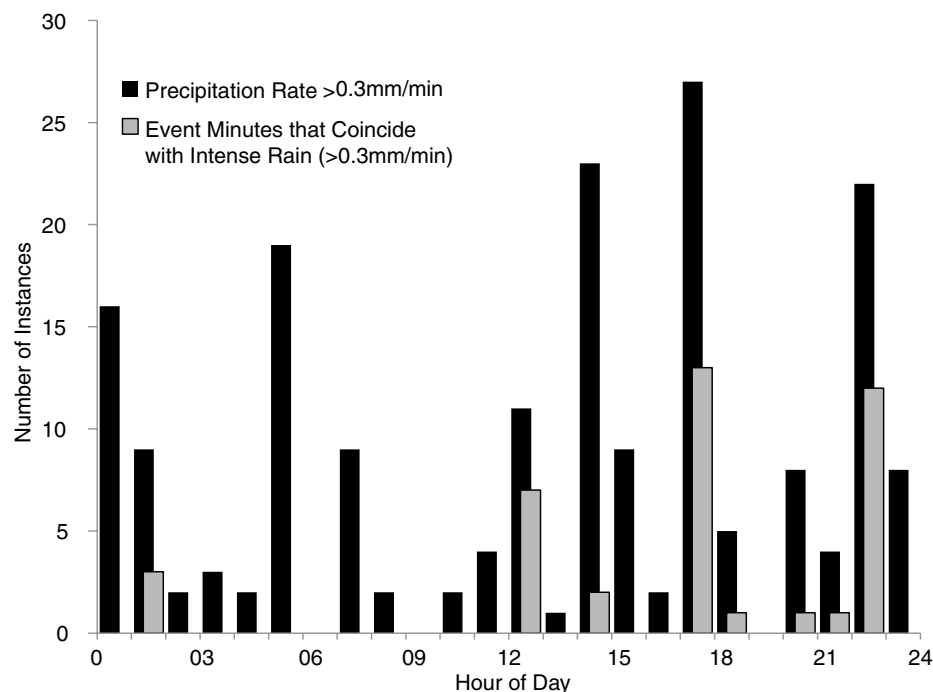
the overall diurnal temperature variation closely (Fig. DR26 [see footnote 1]).

Figure 14 illustrates the corresponding macroscopic thermal stress regime from the model; tension develops in much of the interior of the boulder as the rock surface heats and expands, reaching a maximum around midday. As the rock begins to cool, tension increases near the surface and peaks close to sunset (Fig. 14). These results are similar to those reported for a simpler case of a perfect isotropic sphere subjected to a rotating heat source (Tanigawa and Takeuti, 1983). The model further calculates the distribution of stresses within 3-D slices of the boulder, which shows some directionality with respect to the distribution of maximum stresses; the direction and magnitude of this directionality changes through the day (Fig. DR27 [see footnote 1]).

Importantly, for boulders of about this size (20 cm diameter), simple solar forcing results in significant macroscopic tensile stresses through portions of the boulder during a substantial fraction of each day, and they reach 0.7 MPa, a magnitude likely sufficient to exceed 10–20% of  $K_{Ic}$ , the threshold beyond which subcritical crack growth will occur (Atkinson, 1987). It should be noted, however, that this lower stress limit threshold value,  $K_{Ic}$  (sometimes referred to as the “stress corrosion limit,” a slight misnomer as subcritical crack growth can proceed by other mechanisms in addition to stress corrosion), is not well constrained for rock, and it is well documented to change proportionally to fracture toughness in rocks with differing degrees of weathering, moisture content, or rock chemistry (Brantut et al., 2013).

Moreover, these results possibly under- or over-estimate maximum overall solar-induced stresses in the boulder because this modeling neglects two contributions to the stress: (1) grain-scale thermal stresses, which are expected to be significant in any polycrystalline rock due to differences in the coefficients of thermal expansion of adjacent minerals and due to diurnal temperature ranges (Holzhausen, 1989; Molaro and Byrne, 2015), and (2) stresses arising from complexities in surface temperature, such as those due to passing clouds, storms, and the “weather-related” events that typify many of the event days described herein.

We expect both of these additional stress contributions to be important based on our data showing that the majority of AEs coincide with such weather events, and that the associated surface temperature changes are similar or larger and faster than those on relatively stable weather days such as those consistent with the model input. Furthermore, modeling results (Molaro and Byrne, 2015; Eppes et al., 2015) suggest that grain-scale stresses generally peak at similar times of day as those of macroscale stresses described earlier.



**Figure 13.** Histogram depicting the time of day of all instances of heavy rainfall (intensities  $>0.3$  mm/min) and event minutes that occurred coincident with those instances.

More detailed comparisons will be necessary to determine the extent to which these differing sources of thermal stresses may serve to accentuate, or to offset, each other.

### Solar-Induced Thermal Stresses and Subcritical Crack Growth

#### Conceptual Model

We propose a conceptual model to account for the majority of the rock cracking observed in this study. Simple solar forcing generates thermal stresses sufficient to cause slow subcritical crack growth at certain times of day (Fig. 3). At these times, weather-driven temperature perturbations on the boulder surface can increase the stresses sufficiently to trigger accelerated crack growth because antecedent thermal stresses are already near their peak (Fig. 14). We observe that the thermal conditions necessary for triggering these accelerations in cracking vary in space and time (e.g., Figs. 8–10). We hypothesize that this variation is attrib-

able to a spatio-temporally varying stress field in the rock. The stress field is not only a result of dynamic thermal boundary conditions caused by diurnal solar cycling and rapidly changing weather conditions, but it is also a result of ongoing subcritical crack growth in the boulder itself, which in turn influences stresses and rock properties. Thus, this conceptual model explains why we do not observe specific thresholds in—or simple correlations between—cracking and temperatures, temperature range, or rates of temperature change (Table 1; Figs. DR1 and DR3–DR18 [see footnote 1]).

Calculated macroscopic (Fig. 14) and grain-scale (Holzhausen, 1989; Molaro and Byrne, 2015) thermal stresses associated with simple solar forcing are relatively low and generally below the tensile strength of granite. Because these stresses likely exceed  $K_{th}$ , i.e. 10–20% of cited values for granite's  $K_c$  they are nevertheless likely, by themselves, to be of sufficient magnitude for subcritical crack growth to proceed, albeit at extremely slow rates unmeasur-

able in most laboratory settings ( $<10^{-9}$  m  $s^{-1}$ ; Atkinson, 1984; Atkinson and Meredith, 1987). Thus, we suggest that cracks are propagating subcritically in the boulder via solar-induced thermal stresses even when not measured by our AE system, which was designed to monitor relatively energetic crack growth. Our measurements of daily temperature-dependent cycling of strain and permanent extensional strain, not commensurate with measured AE events, support this conclusion (Fig. 11).

In general, however, when slow-growing microfractures reach a critical length and/or come sufficiently close to one another after extended periods, stresses at crack tips are amplified, thereby accelerating crack growth and coalescence (e.g., Anderson, 2005; Atkinson, 1987). Thus, when microfractures are sufficiently long, small increases in stress are able to greatly increase cracking rates, still at stresses lower than critical  $K_c$  values. Once the stress is relieved along the flaw, or the crack intercepts a grain or inclusion that impedes its growth, however, cracking halts. Then the process of slower, subcritical growth begins again until stresses at the crack tip reach suitable levels to reaccelerate crack growth (e.g., Anderson, 2005).

We therefore hypothesize that periods of AE-measurable crack growth in this study were triggered by both (1) stress perturbations brought on by weather when antecedent solar-induced stresses were already high and (2) sufficient lengthening of cracks by simple solar forcing that in turn lowered stresses necessary for more rapid, measurable growth. For the former, it is important to recognize that the larger the portion of any given elastic body under stress, the larger is the number of inherent flaws that are subject to those stresses, and thus the lower is its overall strength (e.g., Weibull, 1939). Thus, the probability of cracking in any brittle mass, at any given time, reaches a maximum during times when overall tension is high over a large domain. These times are not necessarily when tensile stresses are locally at their maximum. Accordingly, thermal stresses experienced by our rock during weather events would be more likely to induce cracking if they occurred when substantial portions of the boulder were already under considerable tension due to simple solar forcing (e.g. Fig. 14), and not necessarily when thermal stresses were at a peak locally due, for example, to a rapid temperature change. We did note an offset in the timing of calculated peak midday thermal stresses (generally before noon; Fig. 14) and most observed cracking (1 p.m.; Fig. 3). There did not seem to be such an offset in the timing of near-sunset cracking.

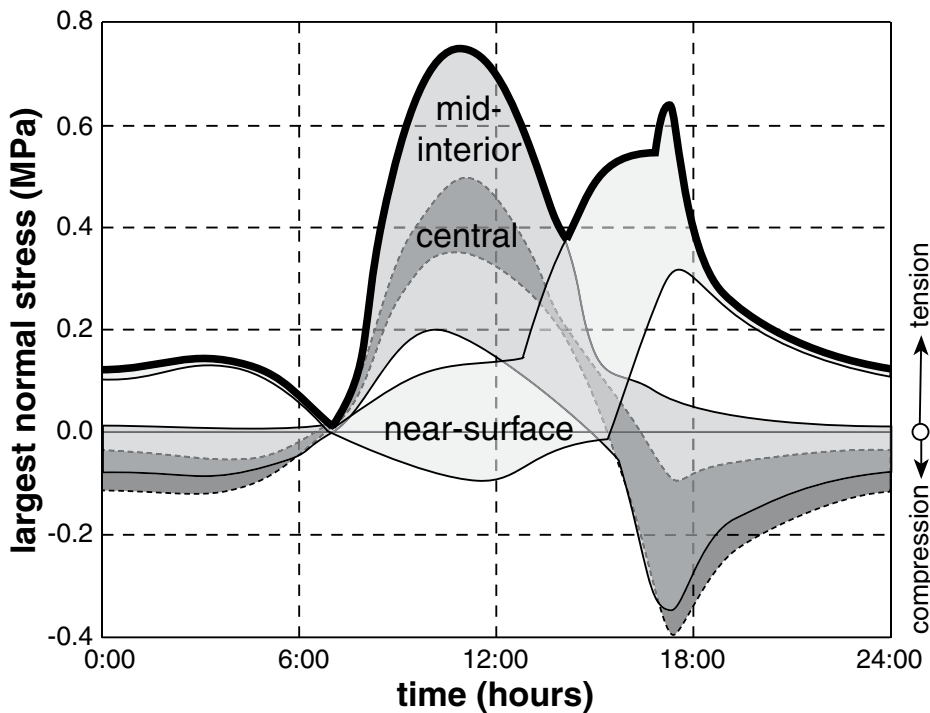


**Figure 14.** Calculated stresses for a spherical ~20-cm-diameter boulder under conditions representative of this study site. Each colored domain represents the stress evolution calculated at one of 78 nodes for three portions of the boulder (near-surface; interior; central); the delimiting lines are the envelopes of the stress fields. Positive values represent tensile stress, which are of greatest interest in the context of fracture activity; negative values represent compressive stress. The heavy black line represents the peak tensile stress experienced anywhere in the boulder. Stresses were calculated assuming a simple diurnal temperature variation associated with insolation (see text). Figure is from modeling developed by Shi (2011).

Our observations of long periods of minimal AE activity punctuated by few periods of rapid crack growth indicated by short-duration large AE clusters (Fig. 2) are consistent with recognized behavior for subcritical crack growth under cyclic loading (Atkinson, 1987) and are similar to AE measured in rock that is failing under cyclic loading conditions (e.g., Xiao et al., 2010). Under these conditions, cracks propagate very slowly and then suddenly accelerate after a number of loading cycles. Furthermore, daily rock strain measured herein, which was not accompanied by AE events, may nevertheless reflect ongoing crack propagation, because such cyclic strain is known to drive subcritical crack growth through fatigue processes (e.g., Costin and Holcomb, 1981).

### *Influence of Weather-Actuated Thermal Stresses*

Because the length and proximity to each other of slowly growing cracks vary at any given time, so too will the stresses necessary to propagate them more rapidly (Anderson, 2005; Atkinson, 1984). For the majority of the AE activity we measured during the monitoring period, those additive stresses appeared to be thermal. Over 90% of AE events described herein occurred during distinct increases in the range of rock surface temperature across the boulder surface, a classic thermal-stress-inducing scenario for elastic solids (e.g., Timoshenko and Goodier, 1970; Fig. 4). In the 5 days with highest numbers of events, the surface temperature range increased by as much as 4 °C within the few tens of minutes of the high AE period (Figs. 8–10). The maximum (between the eight thermocouples) rate of this change for all event times averaged 0.36 °C/min and was significantly greater than the overall average rate of change for the entire record (0.08 °C/min; Table 1).

We suggest that these weather-driven increases in temperature range across the surface of the rock thermally stressed it in much the same way that simple solar forcing generally causes peaks in thermal tensile stresses during times of heating and cooling (Fig. 14). Figure 4 illustrates that the rock regularly experienced peaks and accelerations in rock surface temperature range throughout the day that were of a similar or greater magnitude as those occurring at sunrise or sunset.

Although the onset of cracking characteristically coincided with wind- or moisture-driven changes in temperatures (Fig. 4), there was no correlation between cracking rates and wind speed or precipitation (Figs. DR1 and DR4 [see footnote 1]). Further, the polarity of the temper-

ature change induced by these weather events was not always consistent with that driven by simple solar forcing. In other words, observed cracking sometimes occurred when weather-driven thermal anomalies accentuated antecedent solar-induced thermal stresses, i.e., sudden heating around midday or rapid cooling in the evening (e.g., 5 August 2010 and 14 August 2010; Fig. 10), but not always.

Thus, the stresses arising from complex and significant weather-driven cooling and heating episodes (e.g., Figs. 8–10) combined with the stresses related to simple solar forcing likely result in temporally and spatially varying thermal stresses overall. In turn, these changing thermal stresses likely dictate an ever-changing threshold of additional stress, thermal or otherwise, necessary to trigger cracking at any given time of day, not just those associated with peak insolation-related thermal stresses. We believe that this inherent variance may be why we did not typically observe cracking in association with extremes in environmental conditions (Table 1) or any bivariate correlations between cracking rate and environmental factors like insolation, moisture, temperature rate of change, etc. (Figs. DR3–DR16 [see footnote 1]).

Instead, the primary consistent characteristic of almost all cracking episodes was that they occurred during periods of peak tensile stresses due to simple insolation-related macroscale thermal stresses as well as grain-scale stresses. We observed no similar temporal pattern in any other environmental variable that we examined, including periods of rain, intense rain, high winds, extreme temperatures (Fig. 6), or moisture (e.g., Figs. 5 and 13). When weather-driven temperature variations, similar to those observed to trigger cracking, occurred at times of day characterized by low solar-induced thermal stresses (Fig. 14), they caused little or no AE activity (e.g., Figs. 3, 4, and 13). The most conspicuous exceptions to this observation were events that occurred in the overnight hours (note minor tertiary midnight peak in Fig. 3); however, many of these followed an event cluster that began the previous day (e.g., Fig. 4, 1/11/2011, 3/24/2011, 10/26/2011). Such cracking that continues after a recent major episode of weathering-related fracture is expected (e.g., Stock et al., 2012), because cracking itself results in the transfer of zones of peak stresses, which can in turn trigger subsequent cracking, similar to earthquakes impacting aftershocks by altering the shear and normal stress on surrounding faults (Stein, 1999).

### *Cracking Locations*

The two cracking location clusters we identified, near and at the rock surface (Fig. 12),

are also consistent with our conceptual model for ongoing subcritical crack growth due to insolation-related thermal stresses. These two distinct zones generally coincide with the areas of the boulder that experience maximum solar-induced macroscopic thermal stresses (Fig. 14; Shi, 2011). Modeling results also show, however, a distribution of stresses with nearly spherical symmetry, characterized by only slightly higher tension in the upper hemisphere at midday, and in the southwestern portion of the rock at sunset (Fig. DR27 [see footnote 1]). Our observations of predominantly upper-hemisphere (Fig. 12) and north or eastern quadrant cracking (Fig. DR19 [see footnote 1]) differ from what might be expected given this lack of significant contrast in the distribution of stresses from one portion of the rock to another. We did, however, observe maximum permanent strain and maximum macro-evidence of fracture in the southwestern portion of the rock, indicating that either cracking rates in these locations are too slow to trigger AE events, or AE events were mislocated when they occurred in proximity to the rock “dimple” (see Results); we suspect the latter.

Further, upper portions of the boulder experience the largest range of temperature (e.g., Figs. 8–10), and thus likely experience the largest (Holzhausen, 1989; Molaro and Byrne, 2015), and largest number of, thermal stress perturbations throughout the period of record. This latter effect has been shown in rock cladding to produce greater rock breakdown rates (Gómez-Heras et al., 2008), likely because fatigue-driven subcritical crack growth is dependent not only on the magnitude of the range of the stress loading cycle, but also the number of stress cycles (e.g., Costin and Holcomb, 1981).

Another apparent inconsistency between existing modeling results of the macroscopic state of stress and our data is that there is no substantial difference in the diurnal timing of cracking in the interior of the boulder versus its exterior (Fig. 12C); modeling results (Fig. 14) show that these locations experience peak stresses at different times of day. However, if weather-induced thermal perturbations are opposite in sign to solar-driven ones (i.e., storm-driven cooling at midday), and if the magnitudes of such perturbations were similar to those produced by simple diurnal forcing, tensile stresses might develop simultaneously in both the interior and exterior sectors of the boulder. To date, modeling has only been used to calculate macroscale thermal stresses affected by simple solar forcing in a boulder idealized as a homogeneous elastic sphere. A more detailed examination of AE localizations, combined with modeling that includes additive temperature fields, is needed

to elucidate these effects but is beyond the scope of this paper.

### Comparison with Pilot Rock

Results from the pilot deployment are consistent with our hypothesis that antecedent solar-induced stresses set the stage for triggering cracking by other processes. The pilot rock was placed where, by midmorning, it was shaded by the adjacent building, resulting in no significant midday heating. This lack of direct radiation on the boulder would decrease the maximum midday macroscopic tensile stresses as calculated numerically (Shi, 2011). Such shading during the heat of the day would also decrease the magnitude of grain-scale thermal stresses overall because they are dictated largely by the diurnal range of temperature (Molaro and Byrne, 2015). In this context, it is not surprising that the pilot rock experienced only 55 events total (compared to ~11,000 during a similar 3 mo period for the boulder described in this study), and that cracking in the pilot rock occurred almost exclusively at sunset hours (Fig. DR2 [see footnote 1]), compared to both midday and sunset for this study (Fig. 3). These results underscore the potential effects that topographic shading may have on insolation-related thermal stresses and associated crack growth processes.

### Insight into Thermal Shock Thresholds

As has been demonstrated by the data herein, as well as by other workers (e.g., Gómez-Heras et al., 2006, 2008), the thermal exposure history for any rock exposed at Earth's surface is spatially and temporally complex, even at the scale of a single boulder (Figs. 8–10). Under such thermal stress loading, cracks are thought to propagate via both thermal shock and thermal fatigue (e.g., review in Hall and Thorn, 2014). Thermal shock refers simply to damage associated with a single temperature cycle, whereas fatigue refers to damage that occurs after numerous cycles. The nature of the thermal stresses that impart the damage can be the same. The thermal stresses necessary to damage any given rock by a single cycle, however, decrease with the number of cycles experienced, and such “prestressing” has been shown to greatly reduce the rate of temperature change that can induce thermal shock-driven fracture (Viles et al., 2010). Furthermore, as previously mentioned, as cracks grow in number and size, stresses required for subcritical crack growth will further be reduced (Atkinson and Meredith, 1987). Thus, in a material with such a complex exposure history as naturally exposed rock, thermal shock and fatigue cannot likely be readily separated from one another with respect to

subcritical crack growth. This muddling of processes is not always necessarily the case, however, as single cycles of rapid thermal changes have been observed to produce tell-tale polygonal cracking in laboratory experiments (Hall and Thorn, 2014).

Nevertheless, specific rates of temperature change are commonly cited in the literature as thresholds for inducing “thermal shock cracking” in rocks, and they range broadly from 0.3 °C/min to 44 °C/min (see review in Hall and Thorn, 2014). The most commonly cited value is 2 °C/min for rocks (Richter and Simmons, 1974; Yatsu, 1988). There is, however, little if any documentation to support the existence of this threshold, particularly under commonly experienced temperature ranges at Earth's surface (see review in Boelhouwers and Jonsson, 2013). For example, in an experimental study on a fresh piece of Westerly granite, Yong and Wang (1980) find that below temperatures of ~70 °C, they could not induce cracking (as measured by AE), even at rates of temperature change as high as 12.5 °C/min. Additionally, numerical models demonstrate that, at least at the grain scale, thermal stress maxima do not coincide with periods of fastest temperature change (Molaro and Byrne, 2013). Our observations of rapid rock surface temperature changes with no observed cracking (Table 1) support the conclusions of these studies.

Furthermore, this study provides robust evidence that the commonly cited 2 °C/min cracking threshold rate is unfounded, at least in the case of a naturally exposed boulder. Thermal fluctuation rates measured herein commonly exceeded 2 °C/min (3889 total instances; Fig. DR25 [see footnote 1]) and no events occurred, regardless of whether that rate persisted for multiple minutes or not (Table 1). Such rapid temperature fluctuations may have to be sustained for significant periods in order to induce cracking in rock (Hall and André, 2003); however, we recorded only 4 AE events during the 1139 times when the average rate of change over a prior 10 min window was >2 °C/min.

Our data are consistent, however, with cracking by thermal shock in the sense that damage often occurs within a single episode of relatively rapid temperature change on the surface of the rock. Our data also show that the thermal regimes at times of cracking are commonly complex, and that cracking does not depend on the rate of surface temperature change alone, but on a host of other antecedent conditions, which typically undergo diurnal variations. Thus, we conclude that finding a universal threshold of temperature change that will always crack natural rock is highly unlikely because of the various spatio-tempo-

ral complexities of each rock's unique exposure history, shape, and size.

### Consideration of Additional Contributing Factors to Observed Rock Cracking

#### Freezing Processes

Freezing is the most commonly cited rock breakdown process in geomorphology literature, particularly as related to humid, mid-latitude climates. This breakdown is most commonly attributed to the freezing of water trapped within pores and cracks due to water's 9% volumetric expansion upon freezing. Both cumulative time in subzero temperatures and numbers of freeze-thaw cycles have been hypothesized to contribute to freeze-related cracking. We see no statistical correlations between these factors and cracking in our rock. A few lines of evidence, however, suggest that freezing water is responsible for at least some of the cracking events that we observed. The single significant event cluster (230 events) that was not associated with any obvious thermal forcing occurred below freezing, and overall 17% of all events occurred when at least one thermocouple on the rock surface sensed subzero-degree (Celsius) temperatures. Also, disproportionately high numbers of events occurring during temperatures in the 0 °C to –3 °C range (Fig. 6; Fig. DR18 [see footnote 1]). The timing of observed “freezing,” AE events however, represents <1% of the total time that all eight thermocouples on the rock surface recorded temperatures below 0 °C, simultaneously.

Frost damage to rocks can also arise from thermodynamically driven movement of water into small cracks and the subsequent formation of segregation ice (e.g., Hallet, 2006; Murton et al., 2006; Vlahou and Worster, 2015; Walder and Hallet, 1985). The ideal temperature range for ice segregation-related cracking, the “frost cracking window,” is between –3 °C and –8 °C (Anderson, 1998; Hallet, 2006), with overall slow, sustained cooling leading to higher efficacy of this process (Walder and Hallet, 1985; Murton et al., 2006). The time spent in the frost-cracking window may well be a useful proxy for frost damage (Anderson, 1998; Hales and Roering, 2007), but there is little field evidence to support or refute this hypothesis (e.g., Girard et al., 2013). We observed disproportionately little cracking in the –3 °C to –8 °C surface temperature range (Fig. 6). Only 79 events (0.2% of all events) occurred during minutes when one or more surface temperatures registered in that temperature range (7.3% of the period of record), even when those temperatures persisted consecutively for 1–3 d.

The majority of recorded “freezing events” occurred during the 10–11 January snow and freezing rain weather episode after the rock had been experiencing subfreezing temperatures and snow/freezing rain for about a day (Fig. 9). As was mentioned previously, the timing of a large number of events, coincident with a weather change, sunset, and rock heating, also makes them a candidate for simple solar forcing–related fracture, whereby elevated thermal stresses may have “tipped the bucket” for cracking by freezing-related stresses. Interestingly, the locations of events on these two days differed somewhat from those of most other high-event days during the period of record in that they did not occur in the northern quadrant of the rock (Fig. DR19 [see footnote 1]), the same portion of the rock that was insulated from temperature change during the event cluster, likely due to snowpack (Fig. 9).

Thus, although many events occurred during subfreezing conditions, we have evidence suggesting that thermal cycling might have contributed in some way to most of them. However, given that our study rock was a single, isolated boulder, exposed to full sun, with few preexisting macrofractures, opportunities for water to enter the interior of the boulder and time for ice lens growth were both limited relative to most rocks and exposures in the field. Thus, the overall likelihood of high frost cracking intensity under the conditions of our experiment is low. At a minimum, however, these observations beg the question: Could elevated thermal stresses exacerbate freeze-related weathering by increasing the number of cracks through which water can migrate and in which ice can grow, or by contributing to the state of stress conducive to crack propagation driven by ice growth? Further examination of our AE data might reveal mechanistic differences between events related to freezing and those caused by thermal stresses.

#### **Moisture-Related Processes Besides Freezing**

Numerous studies have documented correlations between rock moisture and physical weathering; however, the mechanistic link between moisture and rock breakdown is not typically explained (e.g., Elliott, 2008; Sass, 2005), particularly beyond its role in stress loading itself. For example, in obvious ways, moisture is necessary for stress loading by freezing or hydration processes. As we have explained here, and as has been observed by others (Griggs, 1936; Viles et al., 2010), we also see evidence in our data that moisture played a key role in stress loading, because it is a primary means by which a rock surface can be rapidly cooled, which induces significant thermal stresses at the rock surface.

In addition, however, it is widely recognized from experimental studies that subcritical crack growth rates are strongly correlated with rock moisture content regardless of the stress-loading mechanism (e.g., Atkinson, 1984; Brantut et al., 2013; Nara et al., 2013), a fact that has rarely, if ever, been explicitly considered by weathering scientists. This effect is due to the fact that subcritical crack propagation, as considered at the molecule scale in rock, often occurs via chemical processes such as stress corrosion (e.g., Atkinson and Meredith, 1981). Given that a disproportionate amount of observed cracking occurred at high relative humidity (Fig. DR18 [see footnote 1]), it is possible that our data indicate that these moisture-dependent subcritical crack growth processes are influencing cracking rates beyond the influence of moisture on any particular stress-loading mechanism. More detailed moisture data, beyond the bimodal wet-dry of our measurements, or numerical modeling would be required to determine the extent to which moisture contributes to subcritical crack propagation by weathering-related stresses.

Nevertheless, the surface of our rock was wet most often in the morning hours (3 a.m. to 10 a.m.), during which the fewest events overall were recorded (1.6%). During 99% of all of the times when the rock surface was wet and AE data were available, no events were recorded. During 45% of all the days for which the rock surface registered moisture during any part of the day, zero events occurred. Thus, overall, our observations suggest that moisture-related processes such as mineral hydration and adsorption are not the principal stress-loading processes driving the AE activity we measured. It is unclear at this time, however, to what extent this conclusion can be generalized because bedrock outcrops are more likely to receive and store moisture than the study boulder, and moisture retention tends to be high in any wooded area that is typically more shaded and that provides more contact with organic-rich, moist soils.

Finally, Moores et al. (2008) have proposed that preexisting rock surface cracks in which the orientations result in greater shading throughout the day and year will remain relatively moist, making them more likely to grow by any water-driven process. If greater retention of moisture in microcracks alone were responsible for the majority of cracks, however, most cracks should grow on the bottom of the rock, where it is most shielded from the drying effects of insolation. It is possible, however, that insolation-related preferred moisture retention combined with insolation-related thermal stresses promote propagation of certain fractures over others due to mois-

ture’s influence on subcritical crack growth rates by stress corrosion and other processes.

#### **Implications for Field-Based Observations of Macrofractures**

Field-based observations of the orientations of macrofractures in boulders found in humid temperate environments similar to that of this study indicate that a majority of these fractures exhibit preferential NE-SW orientations and preferential dip angles of  $\sim 50^\circ$  (Aldred et al., 2015). These preferred crack orientations have also been observed in boulders located in Earth’s deserts and on the surface of Mars and are hypothesized to arise from subcritical crack propagation occurring preferentially at times of day when numerically modeled solar-induced tensile thermal stresses are highest (Eppes et al., 2015). Our data provide direct support of this hypothesis in that we observed cracking to preferentially occur at specific times of day. In turn, the geometry of the temperature fields that arise at these times of day (Fig. 7) is broadly consistent with the orientation of the distribution of maximum thermal stresses calculated by our model (Fig. DR27 [see footnote 1]), both of which are oriented in approximately N-S directions that are similar to measured macrofractures in boulder fields. Finally, the secondary N-S and E-W vector modes of event locations, as measured as a direction from the center of the rock (Figs. DR19 and DR20 [see footnote 1]) are similar to the orientations of measured macrofractures at many individual field site locations (Adelsberger and Smith, 2009; Aldred et al., 2015; D’Arcy et al., 2015; McFadden et al., 2005).

Theory and experiments show that, all things being equal, microfractures preferentially propagate and coalesce into macrofractures in regions where fracture density is highest (Nara and Kaneko, 2006). If the majority of ongoing subcritical crack growth is occurring within specific “slices” of the rock, as we have observed (Fig. DR19A [see footnote 1]), due to the orientations of maximum solar-induced thermal stresses, then it would be expected that developing macrofractures will preferentially form aligned within these densest areas of individual cracking events. Thus, our data provide evidence for the development of an insolation-related microstructure heterogeneity that acts much like a bedding plane or foliation-related zone of weakness, and that can be exploited by other weathering processes or stress-loading mechanisms such as ice segregation. Also, as previously mentioned, cracks in these orientations may also be additionally prone to fracture due to their possible higher moisture content from orientation-related shading (Moores et al., 2008).

## Ongoing and Future Work

A field experiment virtually identical to that described herein has been conducted over a longer period (~3 yr) for a boulder of the same Santa Ana Granite in semiarid south-central New Mexico (Eppes et al., 2012). A detailed examination of the New Mexico data will allow us to determine the extent to which observations are common to all three data sets (North Carolina pilot study, North Carolina study [this study], New Mexico study) and test the hypotheses we have presented. For example, was the lack of cracking in the 5 °C–25 °C surface temperature range (Fig. 6) for the North Carolina rock linked to the weather conditions for that year in that climate, or does it represent a more universal “noncracking window”?

Preliminary analysis from the New Mexico desert deployment (Eppes et al., 2012) indicates that measured AEs are similar in their major temporal and spatial patterns (midday and afternoon, weather-driven, upper-hemisphere cracking dominating the record) to those presented in this study, as well to those measured in the pilot deployment. Therefore, we suggest that the observations discussed herein are generally representative of the overall mechanical deterioration and breakdown of granite boulders exposed to the sun in a range of climates, not just the boulders used in the experiments. Moreover, we suspect that our results also pertain in many ways to other rock types and locations, and to exposures of bedrock. Rates of cracking measured herein might, however, be higher than for finer-grained rocks that are not as susceptible to cracking by granular disaggregation (e.g., Gómez-Heras et al., 2006), and that are also known to persist longer than their coarse-grain counterparts in natural settings (McFadden et al., 1989).

A principal objective of our continuing modeling effort is to define as precisely as possible the state of stress in the boulder at the peaks of AE activity by using thermal boundary conditions similar to the highly transient and complex temperature fields we measured during high-event days. In addition, we will explicitly examine subcritical crack growth processes in the context of the modeled stress field, keeping in mind that as cracks grow, the stress intensity can increase through time even under constant far-field stress. Finally, to complement this numerical work, we also intend to study in detail the spatio-temporal clustering of AE events on high-event days in the context of new modeling results. Overall, these efforts should help to further elucidate the factors that dictate solar-driven mechanical weathering on Earth and other planets.

## CONCLUSIONS

Our continuous, high-resolution monitoring of rock cracking and coincident environmental conditions sheds new light on how insolation-related thermal stresses contribute to rock weathering.

In this study, we closely examined the key factors that drive mechanical weathering under the simple case of a boulder sitting on an unvegetated ground surface. We provided evidence that suggests that solar-induced thermal stresses due to simple diurnal forcing commonly sustain subcritical crack growth, as well as globally elevated background tensile stresses, both of which contribute to rapid crack propagation, especially when tension in the rock is enhanced for other reasons. In the relatively limited number of AE event clusters of this study, those reasons were abrupt thermal perturbations. Our numerical model results show that the specific periods of the day when this cracking occurred were precisely those when the antecedent tensile thermal stresses, at both macro- and microscales in the rock, due to simple, diurnal solar exposure are highest and closest to failure. The relatively sparse number of cracking clusters that occurred over the study period also underscores the relative rarity of conditions that lead to the bulk of the measurable rock fracture activity, and the benefits of such long-term experiments.

Thus, overall our data suggest that simple diurnal solar forcing sets the stage for, and/or contributes to rock weathering in several ways: (1) It recurrently produces thermal stresses in rock sufficient to produce slow, sub-critical crack growth, and also to effectively lower the stress threshold for cracking by other loading mechanisms; (2) it progressively weakens the rock through crack growth, which increases the number and length of cracks that can propagate by any mechanism; and (3) these growing cracks in turn likely enhance weathering overall. For example, they accelerate physical weathering by increasing the stress intensity factor of any given crack, and accelerate chemical weathering processes by increasing the availability of fresh surface area and the transport of reactive fluids.

These observations of weather-driven and sun cycle-related cracking are not new or unique. Whitaker (1974) recounted a large granite boulder split shortly after a storm in association with a “loud explosion,” and anecdotes of hearing noises like “pistol shots” in hot deserts shortly after such storms and/or sunset are common (e.g., Griffiths et al., 2012). Our data and interpretation provide a mechanistic basis for understanding these long-observed phenomena. Furthermore, our data suggest that mechanical

weathering is sensitive to storminess (or climate stability), a property of climate that seldom receives attention in weathering studies.

Finally, data presented herein indicate that cracking is not predictable based on simple mathematical indices such as bivariate correlations of crack activity and temperature or moisture. Thus, these data provide evidence that the commonly cited 2 °C/min thermal shock threshold for rock cracking is likely not applicable under most natural conditions (Boelhouwers and Jonsson, 2013). Further, even with a colder-than-average winter (for North Carolina), our data suggest that freezing, and other moisture-dependent stress-loading processes play minimal roles in boulder cracking under the relatively limited conditions of our study. Together, these results are somewhat analogous to the lack of correlations that have been observed between <sup>10</sup>Be-derived bare rock outcrop erosion rates over much longer, Quaternary time scales, and environmental characteristics like temperature, elevation, precipitation, or evidence of past periglacial activity (e.g., Portenga and Bierman, 2011; Hancock and Kirwan, 2007; Small et al., 1997). Our data speak, therefore, to possible alternative variables that may better explain variations in rock erosion rates, namely, those related to a rock’s susceptibility to subcritical crack growth or to thermal forcing. At a minimum, the data presented herein, together with ongoing modeling and field observations, underscore the potential importance of both subcritical crack growth and solar-induced thermal stresses in contributing to mechanical weathering processes on Earth and elsewhere.

## ACKNOWLEDGMENTS

This material is based upon work supported by the National Science Foundation under grant numbers EAR-0844335, EAR-844401, and EAR-0705277, and by the College of Liberal Arts and Sciences of the University of North Carolina at Charlotte. We would like to thank Haywood Rankin and The Red-lair Nature Preserve for the use of their property for this study. We also wish to acknowledge the important contribution of Eppes’ students: Evan Hinson, Lopita Dash, Damika Jones, Vamsi Alla, Gopi Sundaram, and Suzanne Ching, for their critical and extensive assistance with development and management of the “Pebbles” database. Alex Hohl and Adam Griffith provided visualization assistance with Figure 7. Casey Davenport and Warren Pettee provided key help interpreting meteorological data. Eppes would especially like to thank Richard Gostautas of Mistras Group, Inc., for his invaluable assistance in troubleshooting our acoustic emissions system and data, as well as Drs. Leslie McFadden, Gregory S. Hancock, Greg Stock, David Harbor, John Diemer, and Jamie Molaro for their unwavering enthusiasm for this work and many useful conversations over the years. Similarly, Hallet thanks Alan Gillespie for first opening his eyes to this phenomenon, and Robert Holzworth for exploring the World Wide Lightning

Location Network for lightning activity near our study site. Mackenzie thanks Jian Shi for his early work on numerical simulations of thermal stresses in boulders. We also thank Jan Boelhouzen, T.C. Hales, and Jon Pelletier for their attentive reviews of previous versions of this paper.

## REFERENCES CITED

- Adelsberger, K.A., and Smith, J.R., 2009, Desert pavement development and landscape stability on the Eastern Libyan Plateau, Egypt: *Geomorphology*, v. 107, no. 3-4, p. 178–194, doi:10.1016/j.geomorph.2008.12.005.
- Aldred, J., Eppes, M.C., Aquino, K., Deal, R., Garbini, J., Swami, S., Tuttle, A., and Xanthos, G., 2015, The influence of solar-induced thermal stresses on the mechanical weathering of rocks in humid mid-latitudes: *Earth Surface Processes and Landforms*, doi:10.1002/esp.3849.
- Amitrano, D., Gruber, S., and Girard, L., 2012, Evidence of frost-cracking inferred from acoustic emissions in a high-alpine rock-wall: *Earth and Planetary Science Letters*, v. 341-344, p. 86–93, doi:10.1016/j.epsl.2012.06.014.
- Anderson, R.S., 1998, Near-surface thermal profiles in alpine bedrock: Implications for the frost weathering of rock: *Arctic and Alpine Research*, v. 30, p. 362–372, doi:10.2307/1552008.
- Anderson, T.L., 2005, *Fracture Mechanics: Fundamentals and Applications*: Boca Raton, Florida, CRC Press, 640 p.
- Atkinson, B.K., 1984, Subcritical crack growth in geological materials: *Journal of Geophysical Research—Solid Earth* (1978–2012), v. 89, no. B6, p. 4077–4114.
- Atkinson, B.K., 1987, *Fracture Mechanics of Rock*: London, Academic Press, 534 p.
- Atkinson, B.K., and Meredith, P.G., 1981, Stress corrosion cracking of quartz: A note on the influence of chemical environment: *Tectonophysics*, v. 77, no. 1-2, p. T1–T11, doi:10.1016/0040-1951(81)90157-8.
- Atkinson, B.K., and Meredith, P.G., 1987, The theory of subcritical crack growth with applications to minerals and rocks, in Atkinson, B.K., ed., *Fracture Mechanics of Rock*, Volume 2: London, Academic Press, p. 111–166, doi:10.1016/B978-0-12-066266-1.50009-0.
- Beattie, A.G., 2013, *Acoustic Emission Non-Destructive Testing of Structures using Source Location Techniques*: Albuquerque, New Mexico, Sandia National Laboratories Report SAND2013-7779, 128 p., doi:10.2172/1096442.
- Boelhouwers, J., and Jonsson, M., 2013, Critical assessment of the 2 °C min<sup>-1</sup> threshold for thermal stress weathering: *Geografiska Annaler*, ser. A, *Physical Geography*, v. 95, no. 4, p. 285–293, doi:10.1111/geoa.12026.
- Brantut, N., Heap, M., Meredith, P., and Baud, P., 2013, Time-dependent cracking and brittle creep in crustal rocks: A review: *Journal of Structural Geology*, v. 52, p. 17–43, doi:10.1016/j.jsg.2013.03.007.
- Cohen, D., Hooyer, T., Iverson, N., Thomason, J., and Jackson, M., 2006, Role of transient water pressure in quarrying: A subglacial experiment using acoustic emissions: *Journal of Geophysical Research—Earth Surface* (2003–2012), v. 111, no. F3, p. F03006, doi:10.1029/2005JF000439.
- Costin, L., and Holcomb, D., 1981, Time-dependent failure of rock under cyclic loading: *Tectonophysics*, v. 79, no. 3-4, p. 279–296, doi:10.1016/0040-1951(81)90117-7.
- D'Arcy, M., Roda Boluda, D.C., Whittaker, A.C., and Carpinetti, A., 2015, Dating alluvial fan surfaces in Owens Valley, California, using weathering fractures in boulders: *Earth Surface Processes and Landforms*, v. 40, p. 487–501, doi:10.1002/esp.3649.
- Elliott, C., 2008, Influence of temperature and moisture availability on physical rock weathering along the Victoria Land coast, Antarctica: *Antarctic Science*, v. 20, no. 1, p. 61–67, doi:10.1017/S0954102007000685.
- Eppes, M.C., and Griffing, D., 2010, Granular disintegration of marble in nature: A thermal-mechanical origin for a grus and corestone landscape: *Geomorphology*, v. 117, no. 1-2, p. 170–180, doi:10.1016/j.geomorph.2009.11.028.
- Eppes, M., Warren, K., Hinson, E., and Dash, L., 2012, Long term monitoring of rock surface temperature and rock cracking in temperate and desert climates: Washington, D.C., American Geophysical Union, Fall meeting supplement, abstract EP41F-0848.
- Eppes, M.-C., Willis, A., Molaro, J., Abernathy, S., and Zhou, B., 2015, Cracks in Martian boulders exhibit preferred orientations that point to solar-induced thermal stress: *Nature Communications*, v. 6.
- Garbini, J., 2009, *Instrumentation and Analysis of the Diurnal Processes Affecting a Natural Boulder Exposed to a Natural Environment*: Charlotte, North Carolina, University of North Carolina at Charlotte, 148 p.
- Girard, L., Gruber, S., Weber, S., and Beutel, J., 2013, Environmental controls of frost cracking revealed through in situ acoustic emission measurements in steep bedrock: *Geophysical Research Letters*, v. 40, no. 9, p. 1748–1753, doi:10.1002/grl.50384.
- Gómez-Heras, M., Smith, B.J., and Fort, R., 2006, Surface temperature differences between minerals in crystalline rocks: Implications for granular disaggregation of granites through thermal fatigue: *Geomorphology*, v. 78, no. 3-4, p. 236–249, doi:10.1016/j.geomorph.2005.12.013.
- Gómez-Heras, M., Smith, B.J., and Fort, R., 2008, Influence of surface heterogeneities of building granite on its thermal response and its potential for the generation of thermoclasty: *Environmental Geology*, v. 56, no. 3–4, p. 547–560, doi:10.1007/s00254-008-1356-3.
- Goudie, A.S., 2013, *Arid and Semi-Arid Geomorphology*: Cambridge, UK, Cambridge University Press, 461 p., doi:10.1017/CBO9780511794261.
- Griffiths, J., Fookes, P., Goudie, A., and Stokes, M., 2012, Processes and landforms in deserts, in Walker, M.J. ed., *Hot Deserts: Engineering, Geology, and Geomorphology Engineering Group Working Party Report*: Geological Society of London Engineering Geology Special Publication 25, p. 33–95.
- Griggs, D.T., 1936, The factor of fatigue in rock exfoliation: *The Journal of Geology*, v. 44, no. 7, p. 783–796, doi:10.1086/624483.
- Grosse, C.U., and Ohtsu, M., 2008, *Acoustic Emission Testing*: Berlin, Springer, 406 p., doi:10.1007/978-3-540-69972-9.
- Grossi, C., Brimblecombe, P., Menéndez, B., Benavente, D., Harris, I., and Déqué, M., 2011, Climatology of salt transitions and implications for stone weathering: *The Science of the Total Environment*, v. 409, no. 13, p. 2577–2585, doi:10.1016/j.scitotenv.2011.03.029.
- Hales, T., and Roering, J. J., 2007, Climatic controls on frost cracking and implications for the evolution of bedrock landscapes: *Journal of Geophysical Research—Earth Surface* (2003–2012), v. 112, no. F2, p. F02033, doi:10.1029/2006JF000616.
- Hall, K., and André, M.F., 2003, Rock thermal data at the grain scale: Applicability to granular disintegration in cold environments: *Earth Surface Processes and Landforms*, v. 28, no. 8, p. 823–836, doi:10.1002/esp.494.
- Hall, K., and Hall, A., 1996, Weathering by wetting and drying: Some experimental results: *Earth Surface Processes and Landforms*, v. 21, no. 4, p. 365–376, doi:10.1002/(SICI)1096-9837(199604)21:4<365::AID-ESP571>3.0.CO;2-L.
- Hall, K., and Thorn, C.E., 2014, Thermal fatigue and thermal shock in bedrock: An attempt to unravel the geomorphic processes and products: *Geomorphology*, v. 206, p. 1–13, doi:10.1016/j.geomorph.2013.09.022.
- Hall, K., Meiklejohn, I., Sumner, P., and Arocena, J., 2010, Light penetration into Clarens sandstone and implications for deterioration of San rock art: *Geochronology*, v. 25, no. 1, p. 122–136, doi:10.1002/geoa.20296.
- Hallet, B., 2006, Why do freezing rocks break?: *Science*, v. 314, no. 5802, p. 1092–1093, doi:10.1126/science.1135200.
- Hallet, B., Walder, J., and Stubbs, C., 1991, Weathering by segregation ice growth in microcracks at sustained subzero temperatures: Verification from an experimental study using acoustic emissions: *Permafrost and Periglacial Processes*, v. 2, no. 4, p. 283–300, doi:10.1002/ppp.3430020404.
- Hallet, B., Mackenzie-Helnwein, P., Shi, J., and Eppes, M., 2012, Modeling temperature and stress in rocks exposed to the sun: Washington, D.C., American Geophysical Union, Fall meeting supplement, abstract EP44C-07.
- Holzhausen, G.R., 1989, Origin of sheet structure: I. Morphology and boundary conditions: *Engineering Geology*, v. 27, no. 1-4, p. 225–278, doi:10.1016/0013-7952(89)90035-5.
- Hancock, G. and Kirwan, M., 2007, Summit erosion rates deduced from 10Be: Implications for relief production in the central Appalachians: *Geology*, v. 35, p. 1, p. 89–92, doi:10.1130/G23147A.1.
- Khair, A.W., 1984, Acoustic emission pattern: An indicator of mode of failure in geologic materials as affected by their natural imperfections, in Hardy, H.R., Jr., and Leighton, F.W., eds., *Proceedings of the Third Conference on Acoustic Emission/Microseismic Activity in Geologic Structures and Materials*: University Park, Pennsylvania, Trans Tech Publications, p. 45–66.
- Kirchner, J.W., Riebe, C.S., Ferrier, K.L., and Finkel, R.C., 2006, Cosmogenic nuclide methods for measuring long-term rates of physical erosion and chemical weathering: *Journal of Geochemical Exploration*, v. 88, no. 1-3, p. 296–299, doi:10.1016/j.gexplo.2005.08.060.
- Larsen, I.J., Almond, P.C., Eger, A., Stone, J.O., Montgomery, D.R., and Malcolm, B., 2014, Rapid soil production and weathering in the Southern Alps, New Zealand: *Science*, v. 343, no. 6171, p. 637–640, doi:10.1126/science.1244908.
- Leask, H., and Wilson, L., 2003, Heating and cooling of rocks on Mars: Consequences for weathering: *Lunar and Planetary Institute Science Conference Abstracts*, v. 34, p. 1320.
- Lei, X., Kusunose, K., Rao, M., Nishizawa, O., and Satoh, T., 2000, Quasi-static fault growth and cracking in homogeneous brittle rock under triaxial compression using acoustic emission monitoring: *Journal of Geophysical Research—Solid Earth* (1978–2012), v. 105, no. B3, p. 6127–6139.
- Lockner, D., 1993, The role of acoustic emission in the study of rock fracture: *International Journal of Rock Mechanics and Mining Sciences and Geomechanics Abstracts*, v. 30, p. 883–899.
- Lyons, R., and Austin, S., 2005, Influence of diurnal and seasonal temperature variations on the detection of corrosion in reinforced concrete by acoustic emission: *Corrosion Science*, v. 47, no. 2, p. 413–433, doi:10.1016/j.corsci.2004.06.010.
- McFadden, L.D., Ritter, J.B., and Wells, S.G., 1989, Use of multiparameter relative-age methods for age estimation and correlation of alluvial fan surfaces on a desert piedmont, eastern Mojave Desert, California: *Quaternary Research*, v. 32, no. 3, p. 276–290, doi:10.1016/0033-5894(89)90094-X.
- McFadden, L., Eppes, M., Gillespie, A., and Hallet, B., 2005, Physical weathering in arid landscapes due to diurnal variation in the direction of solar heating: *Geological*

- Society of America Bulletin, v. 117, no. 1-2, p. 161–173, doi:10.1130/B25508.1.
- McKay, C.P., Molaro, J.L., and Marinova, M.M., 2009, High-frequency rock temperature data from hyper-arid desert environments in the Atacama and the Antarctic Dry Valleys and implications for rock weathering: *Geomorphology*, v. 110, no. 3-4, p. 182–187, doi:10.1016/j.geomorph.2009.04.005.
- Meredith, P., and Atkinson, B., 1985, Fracture toughness and subcritical crack growth during high-temperature tensile deformation of Westerly granite and Black gabbro: *Physics of the Earth and Planetary Interiors*, v. 39, no. 1, p. 33–51, doi:10.1016/0031-9201(85)90113-X.
- Molaro, J., and Byrne, S., 2013, Microphysical modeling of thermoelastic stresses on airless surfaces: Lunar and Planetary Institute Science Conference Abstracts, v. 44, p. 1790.
- Molaro, J., and Byrne, S., 2015, Grain-scale thermoelastic stresses and spatio-temporal temperature gradients on airless bodies, implications for rock breakdown: *Journal of Geophysical Research—Planets*, v. 120, p. 255–277, doi:10.1002/2014JE004729.
- Moore, J.E., Pelletier, J.D., and Smith, P.H., 2008, Crack propagation by differential insolation on desert surface clasts: *Geomorphology*, v. 102, no. 3-4, p. 472–481, doi:10.1016/j.geomorph.2008.05.012.
- Morton, D.M., Miller, F.K., Cossette, P.M., and Bovard, K.R., 2006, Geologic Map of the San Bernardino and Santa Ana 30' × 60' Quadrangles: U.S. Geological Survey Open-File Report 2006-1217, scale 1:100,000.
- Murton, J.B., Peterson, R., and Ozouf, J.-C., 2006, Bedrock fracture by ice segregation in cold regions: *Science*, v. 314, no. 5802, p. 1127–1129, doi:10.1126/science.1132127.
- Nara, Y., and Kaneko, K., 2006, Sub-critical crack growth in anisotropic rock: *International Journal of Rock Mechanics and Mining Sciences*, v. 43, no. 3, p. 437–453, doi:10.1016/j.ijrmms.2005.07.008.
- Nara, Y., Yamanaka, H., Oe, Y., and Kaneko, K., 2013, Influence of temperature and water on subcritical crack growth parameters and long-term strength for igneous rocks: *Geophysical Journal International*, v. 193, no. 1, p. 47–60, doi:10.1093/gji/ggs116.
- Portenga, E.W., and Bierman, P.R., 2011, Understanding Earth's eroding surface with <sup>10</sup>Be: *GSA Today*, v. 21, no. 8, p. 4–10, doi:10.1130/G111A.1.
- Rao, G.N., Murthy, C., and Raju, N., 1999, Characterization of micro and macrocracks in rocks by acoustic emission, in *Sotirios J. Vahaviolos, ed., Acoustic Emission: Standards and Technology Update STP1353-EB*: West Conshohocken, Pennsylvania, ASTM, p. 141–155.
- Richter, D., and Simmons, G., 1974, Thermal expansion behavior of igneous rocks: *International Journal of Rock Mechanics and Mining Sciences and Geomechanics Abstracts*, v. 11, p. 403–411.
- Sass, O., 2005, Rock moisture measurements: Techniques, results, and implications for weathering: *Earth Surface Processes and Landforms*, v. 30, no. 3, p. 359–374, doi:10.1002/esp.1214.
- Schlesinger, W.H., and Bernhardt, E.S., 2013, Biogeochemistry: An analysis of global change: San Diego, California, Academic Press, 672 p., doi:10.1093/OBO\_dataset\_home.
- Shi, J., 2011, Study of Thermal Stresses in Rock due to Diurnal Solar Exposure [M.S. thesis]: Seattle, Washington, University of Washington, 103 p.
- Small, E.E., Anderson, R.S., Repka, J.L., and Finkel, R., 1997, Erosion rates of alpine bedrock summit surfaces deduced from in situ <sup>10</sup>Be and <sup>26</sup>Al: *Earth and Planetary Science Letters*, v. 150, no. 3-4, p. 413–425, doi:10.1016/S0012-821X(97)00092-7.
- Stein, R.S., 1999, The role of stress transfer in earthquake occurrence: *Nature*, v. 402, no. 6762, p. 605–609, doi:10.1038/45144.
- Stock, G.M., Martel, S.J., Collins, B.D., and Harp, E.L., 2012, Progressive failure of sheeted rock slopes: The 2009–2010 Rhombus Wall rock falls in Yosemite Valley, California, USA: *Earth Surface Processes and Landforms*, v. 37, no. 5, p. 546–561, doi:10.1002/esp.3192.
- Tanigawa, Y., and Takeuti, Y., 1983, Three-dimensional thermoelastic treatment in spherical region and its application to solid sphere due to rotating heat source: *Zeitschrift für Angewandte Mathematik und Mechanik (ZAMM, Journal of Applied Mathematics and Mechanics)*, v. 63, no. 7, p. 317–324, doi:10.1002/zamm.19830630709.
- Timoshenko, S.P., and Goodier, J., 1970, *Theory of elasticity*: Tokyo, McGraw Hill, 567 p.
- Viles, H., Ehlmann, B., Wilson, C.F., Cebula, T., Page, M., and Bourke, M., 2010, Simulating weathering of basalt on Mars and Earth by thermal cycling: *Geophysical Research Letters*, v. 37, no. 18, p. L18201, doi:10.1029/2010GL043522.
- Vlahou, I., and Worster, M., 2015, Freeze fracturing of elastic porous media: A mathematical model: *Proceedings of the Royal Society of London, ser. A, Mathematical, Physical and Engineering Sciences*, v. 471, p. 20140741.
- Walder, J., and Hallet, B., 1985, A theoretical model of the fracture of rock during freezing: *Geological Society of America Bulletin*, v. 96, no. 3, p. 336–346, doi:10.1130/0016-7606(1985)96<336:ATMOTF>2.0.CO;2.
- Warren, K., Eppes, M.-C., Swami, S., Garbini, J., and Putkonen, J., 2013, Automated field detection of rock fracturing, microclimate, and diurnal rock temperature and strain fields: *Geoscientific Instrumentation: Methods and Data Systems Discussions*, v. 3, no. 2, p. 371–406, doi:10.5194/gid-3-371-2013.
- Weibull, W., 1939, A statistical theory of the strength of metals: *Proceedings of The Royal Swedish Institute for Engineering Research*, v. 151, p. 1–45.
- Whitaker, C.R., 1974, Split boulder: *The Australian Geographer*, 12(6), p. 562–563.
- Xiao, J.-Q., Ding, D.-X., Jiang, F.-L., and Xu, G., 2010, Fatigue damage variable and evolution of rock subjected to cyclic loading: *International Journal of Rock Mechanics and Mining Sciences*, v. 47, no. 3, p. 461–468, doi:10.1016/j.ijrmms.2009.11.003.
- Yaalon, D., 1970, Parallel stone cracking, a weathering process on desert surfaces: *Geological Institute of Bucharest: Technology and Economics Bulletin*, v. 18, p. 107–111.
- Yatsu, E., 1988, *The Nature of Weathering: An Introduction*: Tokyo, Japan, Sozisha, 624 p.
- Yong, C., and Wang, C.Y., 1980, Thermally induced acoustic emission in Westerly granite: *Geophysical Research Letters*, v. 7, no. 12, p. 1089–1092.

SCIENCE EDITOR: CHRISTIAN KOEBERL  
ASSOCIATE EDITOR: JON PELLETER

MANUSCRIPT RECEIVED 11 SEPTEMBER 2015  
REVISED MANUSCRIPT RECEIVED 5 FEBRUARY 2016  
MANUSCRIPT ACCEPTED 1 MARCH 2016

Printed in the USA